

Slip Redistribution onto the Totschunda Fault of Southern Alaska—a Result of a Pacific

Jacob Rosenthal¹

¹Affiliation not available

August 14, 2023

Plate Motion Change at ca. 6 Ma

Jacob L. Rosenthal¹, Paul G. Fitzgerald¹, Jeffrey A. Benowitz², James R. Metcalf², Paul M. Betka³

¹Department of Earth and Environmental Sciences, Syracuse University, Syracuse NY 13244, USA

²Department of Geological Sciences, University of Colorado Boulder, Boulder Co 80309, USA

³Atmospheric, Oceanic, and Earth Sciences Department, George Mason University, Fairfax VA 22030, USA

Corresponding author: Jacob Rosenthal (jlrosent@syr.edu)

Key Points:

We document rejuvenation of the Totschunda fault, a crustal scale strike-slip fault, after a Pacific-Yakutat plate vector change at ca. 6 Ma.

The Totschunda fault became the strand of principal slip due to its new favorable orientation over the northern Eastern Denali fault.

Across the circum-Pacific many major strike-slip faults experienced modifications in response to the ca. 6 Ma Pacific plate motion change.

Abstract

The intersecting Totschunda and Denali strike-slip faults of southern Alaska have been active since at least the Cretaceous. As long-lived structures, the history of deformation along these lithospheric-scale faults can be used to investigate slip distribution between pre-existing fault strands and the transfer of stress inland from plate boundaries due to relative plate motion changes. We apply geochronology (zircon U-Pb) and thermochronology (apatite fission track, zircon and apatite (U-Th)/He) along the southern Totschunda fault and integrate our new data with published regional low temperature thermochronology. U-Pb ages from bedrock samples document Cretaceous gabbroic magmatism and Oligocene Wrangell arc volcanism. New thermochronology data from along the Totschunda fault indicate an increase in rapid cooling, interpreted as exhumation in the Late Miocene that continues until the present. We link this increase in vertical tectonics to Totschunda fault strike-slip motion increasing from ~ 2 mm/yr in the Oligocene to the modern rate of ~ 14 mm/yr at ca. 6 Ma based on palinspastic reconstructions. The Pacific plate-North America plate convergence vector rotated $\sim 18^\circ$ clockwise at ca. 6 Ma resulting in an incoming vector that is preferentially aligned with the pre-existing Totschunda fault. This relative plate motion change and the subsequent alignment of the

Totschunda fault with the Fairweather transform, led to slip-rejuvenation along the Totschunda fault and diminution of strike-slip motion on the northern Eastern Denali Fault. We further suggest in other locations around the Pacific margin the Pacific plate motion change in the Late Miocene also triggered fault system reorganization towards mechanical efficiency.

Keywords: Plate Vector Change, Thermochronology, Alaska, Totschunda Fault, Denali Fault, Fault Reactivation

1. Introduction

Convergent margins often accumulate long-lived lithospheric-scale crustal weaknesses that result from the accretion and dismemberment of terranes (e.g., Wilson, 1965). These mechanical weaknesses frequently manifest as strike-slip faults in oblique convergent settings and slip in response to changing plate boundary conditions (e.g., Powell, 1993; Storti et al., 2003; Najman et al., 2022). The evolution of transform-fault systems is a response, in part, to the orientation of pre-existing faults with respect to variations in plate convergence (e.g., Walcott 1998; McCaffrey et al., 2000). Thus, changes in the orientation of convergence during major plate reconfigurations may modify which faults accumulate strain through geologic time. As fault splays are translated and rotated along a master strike-slip system they can also become preferentially aligned for increased slip accommodation (e.g., Riccio et al. 2014).

Strike slip faults typically have a dip slip component in transpressional settings and thus, thermochronology is often used to document rock cooling along strike slip systems (e.g., Fitzgerald et al., 1995; Benowitz et al., 2014) which can be inferred to reflect periods of partitioned horizontal slip. Exhumation related rapid cooling can also be inferred from kinetic modelling of thermochronology data from strike slip fault corridor sampling transects. Therefore, applying geochronology and thermochronology to rock samples collected along the Totschunda fault integrated with regional geologic constraints presents an opportunity to improve our understanding of the slip distribution on the Denali fault strike-slip fault system and also the mechanisms responsible for slip distribution between the Totschunda and Eastern Denali faults since ca. 52 Ma.

The intersecting Totschunda and Denali faults of Alaska are both interpreted as Cretaceous strike-slip faults that developed across a Mesozoic collisional suture zone with strike-slip reactivation of the suture zone structures (e.g., Churkin et al., 1982; Ridgway et al. 2002; Fitzgerald et al., 2014; Trop et al., 2019, 2020). While plate convergence along the southern Alaska boundary continues, Late Miocene clockwise rotation of the Pacific plate and attached Yakutat microplate relative to North America has influenced tectonics extensively in interior Alaska (e.g., Fitzgerald et al. 1993, 1995; Waldien et al., 2019) and may have drastically modified which faults transfer stress from the plate boundary into interior Alaska. Numerous studies suggest that in response to the Late Miocene Pacific-Yakutat plate motion change, the Eastern Denali fault (Figure 1) has played a diminished role in the transfer of slip from the plate boundary to the continental interior (Waldien et al., 2018; Choi et al., 2021; Allen et al., 2022; Trop et al., 2022; Benowitz et al. 2022a, b). Herein we refer to the Pacific and neighboring Yakutat microplate as the Pacific-Yakutat plate when referencing how the Late Miocene Pacific plate vector change affected Alaska plate boundary conditions.

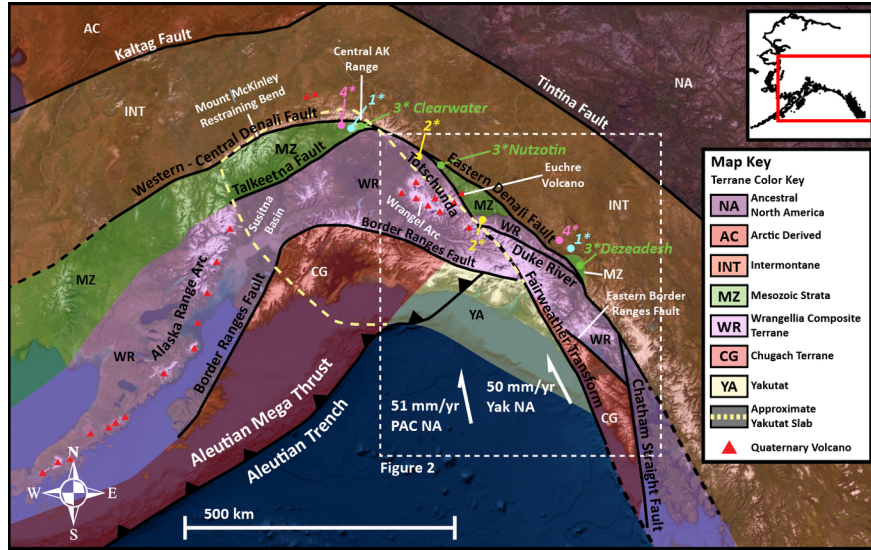


Figure 1: Simplified terrane map of Alaska and the Northern Cordillera with major faults. Most major faults in Alaska are terrane boundary structures (e.g., Coney et al., 1984; Nokleberg et al., 1985). Convergence rates for the Pacific Plate and Yakutat microplate with respect to a fixed north America are from Elliot et al. (2010). Approximate extent of Figure 2 is shown by the white box. Extent of imaged subducted Yakutat microplate is based chiefly on tomography and seismicity data (adapted from Eberhart-Phillips et al., 2006; Bauer et al., 2014; and Wech, 2016; Paulis et al., 2019; Mann et al., 2022). Geologic units modified from Wilson et al. (2015). MZ sediments represent the Alaska Range Suture Zone. Offset Maclaren - Kluane schist shown with blue 1*. Potentially offset Tetelna formation and Station Creek formation shown with yellow 2*. Offset Dezeadesh-Nutzotin-Clearwater basins shown with green 3*. Offset Ruby Range - Susitna Batholith pink 4*.

We present thermochronologic evidence from near-fault and fault-zone bedrock samples along the southern Totschunda fault demonstrating the initiation of rapid exhumation at ca. 6 Ma. We also present geochronology and thermochronology data from cobbles within a nearby basin of Late Miocene-Pleistocene age lying to the east of the Totschunda fault and cut by splays of that fault. Rapid exhumation beginning in the Late Miocene along the Totschunda fault is interpreted as a response to the ca. 6 Ma Pacific-Yakutat plate motion change. This plate motion change led to a more favorable convergence orientation such that slip (with associated exhumation) was primarily accommodated on the Totschunda fault, effectively abandoning strike-slip on the northern Eastern Denali fault. Our results build upon our understanding of how plate boundary forces are transferred and distributed inboard onto strike-slip fault systems like the San Jacinto-San Andreas faults in California (Spotila et al. 2001; Blythe et al., 2002). Furthermore, this data provides insight into long-term slip distribution along strike slip fault systems which can improve seismic hazard forecasts in Alaska and other regions with long lived strike-slip faults and evolving plate boundary conditions (e.g., Alpine fault, Dead Sea, San Andreas fault).

2. Geologic Background

2.1 Alaska Range Suture Zone and the Totschunda-Denali Fault system

The complex Mesozoic to Cenozoic Alaska Range suture zone lies between the peri-Laurentian Yukon-Tanana composite terrane to the north (intermontane terranes) and the more recently accreted, late Paleozoic and Mesozoic intra-oceanic plateau and volcanic arc rocks of the accreted Wrangellia composite terrane (insular

terrane) to the south (Figure 1; Coney et al., 1980; Nokleberg and Richter, 2007; Dusel-Bacon et al., 2013; Jones et al., 2017). Rocks within the Alaska Range suture zone consist primarily of Late Jurassic to Late Cretaceous marine sedimentary strata and associated metamorphic equivalents (Figure 1) (Ridgway et al., 2002; Manselle et al., 2020). The section of the suture zone where parts of this study were conducted is bounded to the north by the near-vertical Denali fault and the Totschunda fault to the south (e.g., Richter, 1976; Allam et al., 2017).

The ~2000 km long, dextral strike-slip Denali fault system is the northern boundary of the Alaska Range suture zone in our region of study and has likely been active since at least ca. 70 Ma (Cole et al., 1999; Miller et al., 2002; Benowitz et al., 2014; McDermott et al., 2019) with ~480 km of documented slip occurring since ca. 52 Ma. The ~480 km of offset since 52 Ma is based in part on the correlative offset ca. 57 Ma. Ruby Range-East Susitna Batholiths (Figure 1; Riccio et al., 2014) and offset ca. 52 Ma Shakwak-Ann Creek Plutons (e.g., Waldien et al., 2021a). These plutons are located within and immediately adjacent to the Maclaren-Kluane schist which is the principal piercing point on the Denali fault (Figure 1). The Maclaren schist and these younger 57 and 52 Ma plutons have been displaced ~480 km from their correlative piercing points (e.g., Forbes et al., 1974; Waldien et al., 2021a). Furthermore, the Mesozoic Clearwater-Nutzotin-Dezadeash Basin complex has been dissected and slivered with the Clearwater sliver being displaced ~480 km from the Dezadeash basin and the Nutzotin sequence being displaced ~360 km from Dezadeash basin (Figure 1) (e.g., Eisbacher, 1976; Lowey et al., 2019; Waldien et al., 2021a).

Because the Maclaren schist and Kluane schist are correlative and have been separated by the Denali Fault, the Maclaren schist cannot be translated down the Totschunda fault and must be restored only to the junction of the two faults (so this translated crustal block can be restored on the Eastern Denali fault to the Maclaren's paleo-connection with the Kluane schist). Currently, the Maclaren schist has been translated roughly 125 kms away from the Totschunda-Denali fault intersection. Since the separation has occurred since 52 Ma, this piercing point provides a limit of 125 kms of horizontal displacement of the Totschunda fault since 52 Ma. Additionally, the Clearwater metasediments have been displaced ~125 km from the correlative Nutzotin Basin (Figure 1) providing an additional piercing point with a nearly identical displacement (Waldien et al., 2022). We therefore infer the Totschunda fault has contributed ~125 kms of the 480 km total displacement of the Maclaren schist (e.g., Eisbacher, 1976; Waldien et al., 2021a; Allen et al., 2022; Trop et al., 2022; this study). Palinspastic restoration of offset volcanic products of the Wrangell volcanic field along the Totschunda fault provide additional markers that suggest ~85 km of the ~125 km of slip occurred since ca. 6 Ma (Berkelhammer et al., 2019; Trop et al., 2022). More speculatively, there is an apparent ~80 km offset (age unknown) of the Border Ranges fault system along the dextral Art Lewis fault (Bruhn et al., 2004; 2014) which is a southern segment of the Connector fault (Figure 1). This Connector fault offset observation is consistent with the offset constraints along the Totschunda fault (Trop et al., 2022).

Besides the dissected Wrangell arc, piercing points that inform on the long term (10^6 years) slip rates along the Totschunda fault are lacking. MacKevett (1978) suggested that the Station Creek Formation just north of the Duke River fault and the Slana Spur Formation/ Tetelna Volcanics near the Totschunda-Denali intersection are possibly correlative based on age (Permian), lithology (interlayered meta-volcaniclastic sediments and lava flows), and similar stratigraphy (Figure 1). These geologic units are separated by ~180 km, but modern dating techniques, detailed mapping, and compositional analysis have not yet been applied to these rocks to corroborate this interpretation.

Using surface exposure ages on offset geomorphological features, Matmon et al. (2006) and Haeussler et al. (2017) determined Pleistocene-Holocene slip rates along the Denali fault system. West of the Totschunda-Denali fault intersection average slip rates on the Denali fault were determined to be ~12.9 mm/yr, east of the intersection ~5.3 mm/yr, and ~7.4 mm/yr along the Totschunda fault. Using field observations, high-resolution imagery, digital elevation models, and cosmogenic nuclide dating, Marechal et al. (2018) document different Pleistocene-Holocene slip rates for the Totschunda and Eastern Denali faults. Marechal et al. (2018) determined rates of ~14.6 mm/yr on the Totschunda fault as compared to <1 mm/yr for the northern Eastern Denali fault (Figure 2). This discrepancy in Pleistocene slip rates for the Eastern Denali

Fault and Totschunda fault reported by Matmon et al. (2006) and Marechal et al. (2018) is not easily explained, but the two research groups did not make slip observations at the same locations. Matmon et al. (2006) made slip determinations based on offset features within ~ 30 km of the Totschunda-Denali fault junction. Marechal et al. (2018) made slip determinations along the entire length of the Eastern Denali fault and note that further than 80 km from the Totschunda-Denali junction, there is no observed horizontal motion on the Eastern Denali fault. Marechal et al. (2018) sampled the Totschunda fault ~120 km south of the Totschunda-Denali fault intersection. We prefer the Marechal et al. (2018) determinations because they align with the long-term geologic record (Waldien et al., 2018, 2021a and Allen et al., 2022) and seismology modeling (Oglesby et al., 2004; Choi et al., 2021).

-Richter and Matson (1971), using offset geomorphological features of unknown age (probably Pleistocene) inferred ~10 kms of slip on the Totschunda fault since ca. 1 Ma. Although this Pleistocene slip rate on the Totschunda (~10 mm/yr) is not well constrained, this constraint is similar to the Holocene rate (~14.6 mm/yr) suggested by Marechal et al. (2018). There is also significantly less seismic activity along the Eastern Denali fault compared to along the Totschunda fault (Figure 2). A compilation of regional thermochronology data (Figure 2) show a pattern of young apatite Helium ages (AHe) along the margins of the Fairweather fault, the inferred Connector fault, and to the north (our data) along the southern Totschunda fault. This data also shows a relative absence of young AHe ages on the southern Eastern Denali fault. Additionally, the 2002 7.9M Denali fault earthquake ruptured the Totschunda fault not the Eastern Denali fault due to the fault's preferential geometry with regards to the regional stress field (Oglesby et al., 2004) adding credence to the Totschunda being the strand of principal slip. We interpret these patterns to further support the Totschunda fault being the primary structure transferring stress inboard from the plate margin since the Late Miocene as compared to the Eastern Denali fault.

Despite most of the lateral displacement on the Totschunda fault occurring since 52 Ma, the fault is likely a Cretaceous structural feature. The Totschunda fault forms part of the inboard suture of the Wrangellia composite terrane with North America as shown by geological mapping (e.g., Richter et al., 1976; MacKevett et al., 1978) and magnetic maps of the region (Bankey et al., 2002). Receiver function analysis from Allam et al. (2017) show a 10 km moho offset across the Totschunda fault (deeper to the west). Regional Wrangell composite terrane (intermontane) suturing along the Totschunda fault by ca. 117 Ma has also been suggested by the presence of well-dated subaerial sedimentary units with dinosaur footprints that unconformably overlap both the Wrangell composite terrane and the Cretaceous Nutzotin basin (Fiorillo et al., 2012; Trop et al., 2020). Trop et al. (2020) infer that since these overlap assemblage rocks preserve land-based fauna, and cover both Wrangellia and the inferred sutured basin, they must record a minimum suturing age. There is also thermochronologic evidence along the central Totschunda fault of a Cretaceous rapid cooling episode which has been interpreted as exhumation during Cretaceous suturing (Milde, 2014; this study) and a dikelet has been dated to ca. 114 Ma ($^{40}\text{Ar}/^{39}\text{Ar}$ K-feldspar) that was injected into pre-existing fault gouge along the Totschunda fault zone (Trop et al., 2020).

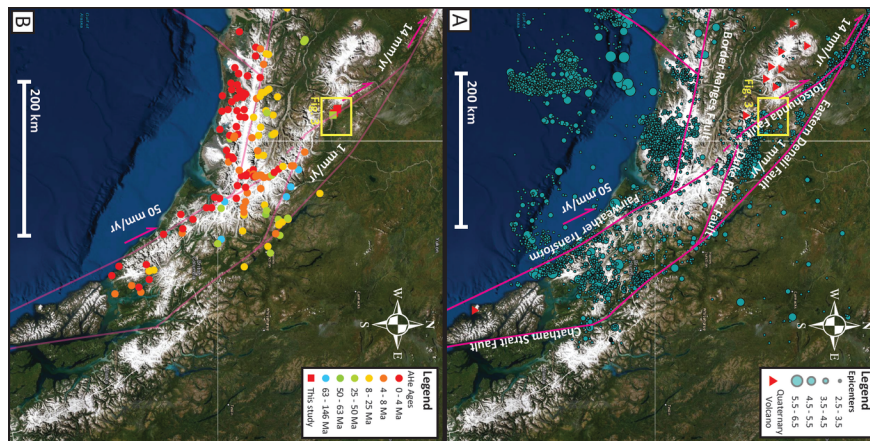


Figure 2: a) Seismicity ranging from 0 to 15 km of depth from 1960 to present-day: Seismic events denoted as blue dots (USGS Earthquake Database). Faults are delineated with solid pink lines and labeled with white lettering. b) Published (see Supplementary File 18) and new apatite (U-Th)/He ages for southern Alaska, listed alphabetically: Enkelmann et al. (2017), McAleer et al. (2009), McDermott et al (2019), Spotila et al. (2004), Spotila and Berger (2010). Major faults shown as semi-transparent pink lines; these are labeled in (a). Approximate slip rates of the major faults shown in white lettering with pink arrows denoting primary sense of slip on each structure. These modern slip rates are from Marechal et al. (2018) and Brothers et al. (2020). Approximate Figure 3 outline shown with yellow box.

The injection of a dike at 30 Ma into the Totschunda fault zone and hypabyssal dikes ca. 25-23 Ma emplaced proximal to, but only on the west side of the Totschunda fault implies fault movement and transtension during the Oligocene (Brueseke et al., 2019). Additional dacitic and andesitic porphyry of Oligocene age along the southern Totschunda fault (this study) also implies Oligo-Miocene slip on the Totschunda fault. Lastly, Milde (2014) collected and analyzed two apatite fission track samples from Cretaceous plutons near the central Totschunda fault and far away (>10 km) from any large Oligocene magmatic bodies that indicate rapid cooling in the Late Oligocene. Milde interprets that these samples were rapidly exhumed in the Late Oligocene on the basis of the presence of Oligocene ages on the west side of the Totschunda fault and Cretaceous ages on the east side of the Totschunda fault.

The restoration of translated Oligocene-Early Miocene boulder conglomerate packages onto the Totschunda from the Central Denali fault (Allen et al., 2022) and coeval focused magmatism along the Totschunda fault (Trop et al., 2022, this study) further support Totschunda fault motion in the Late Oligocene. 23-19 Ma intra-arc extension magmatism in the Sonya Creek Volcanic Field has also been linked to coeval motion along the Totschunda and Eastern Denali faults (Berkelhammer et al., 2019). Intra-arc extensional basin formation and magmatism west of the southern Totschunda fault at ca. 13-5 Ma has also been linked to inferred motion on this structure (Trop et al., 2012). The ca. 10-2 Ma Frederika Formation (White River ‘Tillites’) in a small basin abutting the southern Totschunda fault (e.g., Eyles and Eyles, 1989) are discussed in the next section (2.2) as the formation of that basin is also interpreted to reflect slip on the Totschunda fault in the Late Miocene-Pleistocene. Lastly, the Euchre Volcano erupted directly from the Totschunda fault (Brueseke et al., 2019; Trop et al., 2022) providing indirect evidence of slip and extension in the late Pliocene (ca. 3 Ma).

Northwest of the Totschunda fault, the central Denali fault has acted as a conduit for magmatism since at least the Late Cretaceous based on generally continuous magmatism from ca. 95 to 25 Ma, both proximal to, and directly along the main fault trace (e.g., Regan et al. 2020, 2021; Benowitz 2022a). Likewise, the Totschunda and Duke River faults (which intersect at the southern terminus of the Totschunda fault; Figures 1, 2) appear to have acted as conduits for Wrangell arc magmatism since ca. 30 Ma (Trop et al., 2022, this study). The Duke River and Totschunda faults have probably been connected since Cretaceous times (Cobbett et al., 2016; Trop et al., 2020) with slip at times apparently being transferred from the Duke River onto the Totschunda (Marechal et al., 2018; Choi et al., 2021). Hence, the deformation history of the Duke River fault potentially informs on the deformation history of the Totschunda fault. Eocene to Miocene strike-slip related basins (Ridgway and Decelles, 1993) and Miocene leaky transform magmatism (Skulski et al., 1992; Cole and Ridgway 1993; Trop et al., 2022) along the Duke River fault suggest the Duke River fault was active during most of the Cenozoic. Therefore, it is possible that slip was transferred from the Duke River to the Totschunda from the Eocene to the present (e.g., Marechal et al., 2018) but direct geologic evidence for Eocene -slip along the Totschunda fault is lacking.

2.2 White River ‘Tillites’

The White River ‘Tillites’ were deposited in a small transtensional basin immediately east of the Totschunda fault. This basin contains diamictites and debris flow deposits with interlayered lavas and tuffs derived from the Wrangell volcanic arc (Figure 3). Eight K-Ar whole rock ages from selected tuffs and volcanic flows interbedded in these sediments range in age between 10 and 2 Ma indicating that the sediments were

deposited from Late Miocene to Pleistocene (Denton and Armstrong, 1969). Sediments in this basin are considered part of the Frederika Formation which is also found outside the field area to the south of the Wrangell mountains (MacKevett 1978; Trop et al., 2012; Figure 3). Deposition of the ‘tillites’ are interpreted as being syn-tectonic with slip along the Totschunda fault (Eyles and Eyles, 1989; Trop et al., 2012) based on observed “proximal-sedimentation and a sustained and plentiful supply of coarse debris in a high relief environment” and the possibility that some large debris flows in the section were earthquake derived. The sediments of the White River Tillites are also crosscut and deformed by thrust splays from this fault system. Apatite fission track ages on cobbles from this basin were collected to inform on the provenance and/or the subsequent exhumation history of the basin.

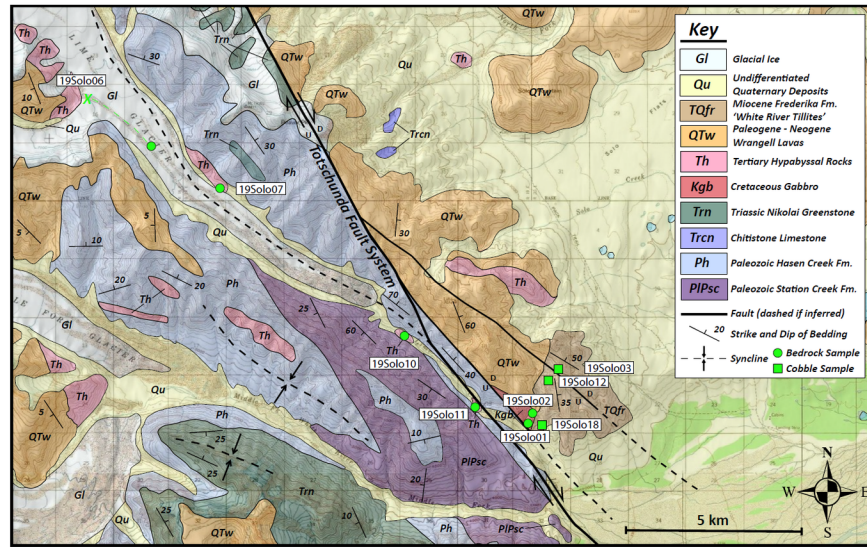


Figure 3: Geologic map of Lime Creek field area with sample locations (Map is adapted from MacKevett (1978) where detailed unit descriptions are recorded). For sample 19SOLO06, the dashed green line leading away from the sample location denotes inferred sample path for a rock that clearly originated from the outcrop denoted with a green X.

2.3 Yakutat Flat Slab Subduction, The Wrangell Arc, and the Pacific Plate

The Yakutat microplate is an 11-30 km thick oceanic plateau, with a dip and crustal thickness contrast between the eastern and western segments and thinning slab thickness towards the north (Ferris et al., 2003; Rossi et al., 2006; Worthington et al., 2012; Mann et al., 2022). The Yakutat microplates convergence angle reflects Pacific plate vector changes through time (e.g., McAleer et al., 2009). The thick (>11 km) Yakutat slab extends for ~250 km northwestward beneath Alaska at a subduction angle of ~20° before the dip angle increases to ~60° beneath the Alaska Range. Seismic images by Ferris et al. (2003) showed that thickened crust of the Yakutat terrane carries through to the steeper slab section to depths of at least 150 km beneath the Alaska range (Mann et al., 2022).

The Wrangell volcanic arc, which is related to subduction of the Yakutat slab, initiated by ca. 30 Ma (Brueseke et al., 2019; Berkelhammer et al., 2019; Trop et al., 2022), coeval with the cessation of magmatism in the Alaska Range arc (Trop et al., 2019; Regan et al., 2021; Benowitz et al., 2022a). This change in location of arc magmatism, from the west to the east has been linked to the commencement of Yakutat flat-slab subduction under southern Alaska (Richter et al., 1990; Trop et al., 2019; Jones et al., 2021). Other upper plate proxies such as exhumation in the Alaska Range (Benowitz et al., 2011, 2012, 2019; Riccio et al., 2014; Lease et al., 2016), deformation of the Susitna Basin (Shaw et al., 2020) and modification of Alaska’s

southern margin forearc (Finzel et al., 2015; Betka et al., 2017; Rosenthal et al., 2018; Pavlis et al., 2019) have also been linked with the initiation of Yakutat flat-slab subduction.

A significant Alaska plate boundary change occurred at ca. 25 Ma, when the Pacific-Yakutat plate vector relative to North America underwent 8° - 15° of counter- clockwise rotation (Jicha et al., 2018). Inboard of the plate margin, this relative plate margin change resulted in significant oblique convergence across the Denali fault system as southern Alaska moved to the northwest (e.g., Benowitz et al., 2014; Trop et al., 2019). A 18° clockwise rotation in convergence angle and a 37 % increase in convergence rate between the Pacific-Yakutat plate relative to North America at ca. 6 Ma (Engebretson et al., 1985; Doubrovine and Tarduno, 2008; Austerman et al., 2011) further increased the northwestward-directed motion of southern Alaska. Fitzgerald et al. (1993, 1995) correlated this plate motion change with a significant pulse of Late Miocene uplift and exhumation in the central Alaska Range, that in combination with the coeval formation of the Mount McKinley restraining bend (Benowitz et al., 2022b) formed the present-day high-standing mountains of the central Alaska Range (Denali; 6190 m). This Pacific-Yakutat plate motion change is also assumed to result in the transfer of slip onto the Totschunda fault from the Denali fault (Waldien et al., 2018; Choi et al., 2021; Allen et al., 2022).

3. Methods and sampling strategy

Strike-slip faults often have a dip-slip component (e.g., Barth et al., 2014) and variations in strike and geometry can result in linked contractional structures (Sylvester 1988; Spotila et al., 1998). Thermochronology presents a means to record the path of a rock as the rock cools and approaches the surface (exhumation), hence a rock sample’s cooling trajectory can be used as a proxy for deformation and a means to unravel the vertical component of the partitioned slip history of strike-slip faults such as along the Alpine Fault of New Zealand and the Fairweather Fault (e.g., White and Green, 1986; Batt et al., 2004; Lease et al. 2021). Provided that the derived cooling ages and modelled cooling paths do not correspond to known regional magmatic ages, by applying thermochronology to samples collected along both sides of the Totschunda fault we can evaluate the cooling and exhumation histories of rocks along the structure and infer changes in slip rates through time.

Rocks in the field area are largely composed of Late-Paleozoic island-arc rocks of Wrangellia Composite Terrane affinity (MacKevett, 1978). These rocks are primarily Permian fossiliferous shallow marine clastic sedimentary rocks and limestones of the Hasen Creek Formation, and volcanoclastic rocks, lavas, and graywackes of the Station Creek Formation (Figure 3). Intrusive rocks in our field area are limited to a Cretaceous (previously mapped as Triassic) gabbro intrusive body on the east side of the Totschunda fault, and many small (<3 km²) Oligocene shallow intrusive andesitic and dacitic porphyry plugs associated with the Wrangell arc. The presence of these andesitic and dacitic porphyry plugs, which are interpreted as hypabyssal rocks (MacKevett, 1978), on the surface suggests 2-3 km of exhumation since their emplacement, making them a reasonable target for thermochronology. Thus, our primary targets for sampling and analyses were these intermediate hypabyssal plugs.

3.1 U-Pb Zircon

We undertook U-Pb dating on zircon to determine the timing of intrusion for magmatic rocks along the Totschunda fault as well as the age of the cobbles in the White River tillites. We performed Laser Ablation Induced Coupled Plasma Mass Spectrometry using an Agilent 7900 ICP-MS and a Photon Machines G2 with a Helix 2 sample cell at the University of Rochester (e.g., Trail et al., 2017). Zircon separates were obtained during the mineral separation processing for apatite using standard mineral separation procedures. Grains were mounted in epoxy and then polished. The mounts were then carbon coated and photographed on the Cameca SXFive Microprobe at Syracuse University using the cathodoluminescence detector. These photos were used to assess crystal zoning and heterogeneity within grains and between samples. Spot locations were

chosen by identifying crystal regions visibly free of inclusions. Zircons were ablated with a spot size ranging from 10 to 35 μm (Trail et al., 2017). The ICP-MS signals were evaluated with the Iolite 3.x software package to select time intervals that reflected the bulk of the zircon grain and avoided sections where the laser ablated through the grain and into the epoxy below, encountered an inclusion, or encountered surface contamination (Paton et al., 2010, 2011). We used the R33 zircon standard (419 Ma) for age correction ablating one R33 zircon for every 10 unknowns with at least one shot between samples (Black et al., 2004). We attempted 20-25 grains or spots per sample. Drift was corrected for using the NIST standard at one shot for every 10 unknowns with at least one shot between samples. Almost all our samples appeared to have some surface lead contamination from processing (potentially from milling or removal of sulfides using nitric acid) and so our time series selections for uranium lead ratios largely excluded the first few seconds of measurements. Additionally, on some grains, we encountered apparent inclusions or would ablate through the grain, and so those shots and times were also excluded. Isotope ratios, dates, and associated uncertainties are calculated from the integrations using the U_Pb_geochronology3data reduction scheme (Paton et al., 2010). The results are summarized in Table 1, S1, & S2.

3.2 Apatite Fission Track Thermochronology

Apatite fission track (AFT) thermochronology has a thermal sensitivity from ca. 120°C to 60°C (e.g., Gleadow et al., 1983; Reiners and Brandon 2007). Above these temperatures fission tracks anneal instantaneously over geologic time and below these temperatures, fission tracks essentially cease annealing over geologic time. The zone between the 120-60°C temperature range where tracks are annealed progressively more slowly as temperature decreases is known as the partial annealing zone (Gleadow and Fitzgerald, 1987). The relative proportions of confined fission track lengths provide information on the thermal history of the sample such as the timing and rate of cooling through the partial annealing zone or partial annealing due to reheating (Gleadow et al. 1986). For example, a track length distribution where almost all tracks are >14-16 μm in length reflects rapid cooling with little to no residence time in the partial annealing zone. More complex track length distributions containing both long and short tracks reflect slow cooling through the partial annealing zone or partial annealing due to reheating with later rapid cooling (e.g., Gleadow et al., 1983; 1986).

The density of spontaneous fission tracks in etched apatite crystals relative to the [U] concentration of individual grains measured using induced fission tracks following irradiation (the external detector method) is used to determine an AFT age (e.g., Hurford and Green, 1983). The composition of apatite plays a role in the annealing of fission tracks; in general tracks in Cl-rich apatite are more resistant to annealing compared to those in Fl-rich apatite (e.g., Gallagher et al., 1998; Ketcham 2007). We collected age and confined track length data including a kinetic parameter that approximates chemical composition (Dpar) and angle of each track with respect to the C-axis of each grain (Donelick et al., 2005). We applied AFT thermochronology to bedrock samples along the Totschunda Fault and to detrital cobbles from the White River ‘Tillites.’ Thermochronology applied to bedrock bounding the Totschunda fault provides potential insight into fault slip related exhumation. In contrast, thermochronology applied to cobbles can provide information on their provenance and pre-deposition cooling (exhumation of the source region) or the burial and subsequent exhumation history of the basin provided the sediments were sufficiently buried to reset the tracks (e.g., Beamud et al., 2011; Fitzgerald et al., 2019). AFT analyses (Table 2) were undertaken at Syracuse University with details given in S14.

3.3 Apatite and Zircon (U-Th)/He dating

Helium analyses were conducted at the University of Colorado in the Thermochronology Research and Advanced Instrumentation Laboratory using an ASI Alphachron for He extraction and measurement (e.g., Flowers et al., 2023a). Individual grains are placed in Nb-tubules, lasered to heat the grain and extract gas, which is spiked with ^3He , purified with SAES getters, and analyzed on a Pfeiffer Balzers QMS quadrupole mass spectrometer. The process is then repeated to evaluate if there was complete extraction of ^4He from

the crystal (e.g., Farley, 2002; Flowers et al., 2023a). Grains are retrieved and then dissolved in nitric acid before being analyzed for U, Th, and Sm using an Agilent 7900 Quadrupole ICP-MS. Grains were picked to avoid broken ends, zoning, inclusions, fractures, and obvious radiation damage to limit the possibility of excessive He from zircon inclusions or He loss from radiation damage and avoid diffusion properties that may result in overdispersion of single grain ages (e.g., Fitzgerald et al., 2006; Flowers et al., 2023b). Grains of adequate size ($> \sim 70$ microns a-axis) are selected to minimize the F_T correction. See Supplementary Files 4, 5, and 6 for more detailed information on zircon and apatite (U-Th)/He dating.

3.4 Multi Kinetic Modelling

Thermochronology data from individual samples were modelled using HeFTy v. 1.9.3 (Ketcham 2005). Inputs to HeFTy are AFT single grain ages, c-axis projected confined lengths, Dpar-, single grain zircon (U-Th)/He (ZHe) and apatite (U-Th)/He ages, and zircon (U-Pb) age constraints when available. HeFTy uses a Monte Carlo approach, generating model AFT age and track length distributions and modeled ZHe and apatite AHe diffusion profiles that are then compared to the measured data using a GOF criteria. Good and acceptable fits are (0.05 and 0.50 respectively). Model paths are allowed to explore temperature-time space (with both cooling and heating path segments) at random intervals. See Supplementary File 7 for more details about the criteria used during thermal modeling.

4. Results and Interpretation

4.1 Geochronology and Thermochronology

We sampled bedrock along the west and east sides of the Totschunda fault on several mapped and previously unmapped small hypabyssal plugs and a small Cretaceous gabbro body (Figures 3, 4). Sample 19SOLO06 was collected from a lateral moraine just downstream from a prominent outcrop of hypabyssal intrusive where this sample clearly originated based on lithology and travel trajectory (Figures 3, 4). U-Pb LA-ICP-MS zircon dating was performed on four of the six bedrock samples from the Lime Creek drainage, and seven of the eight detrital cobbles (Figures 3, 4, 5, 6). We report 14 AFT analyses: six from bedrock samples and 8 from cobbles from the White River ‘Tillites’ (Figures 3, 4, 5, 6). (U-Th)/He analyses were undertaken on apatite separates from 6 bedrock samples (6 grains per sample) and one zircon separate from a bedrock sample (19SOLO02; 3 grains) from the Lime Creek area.

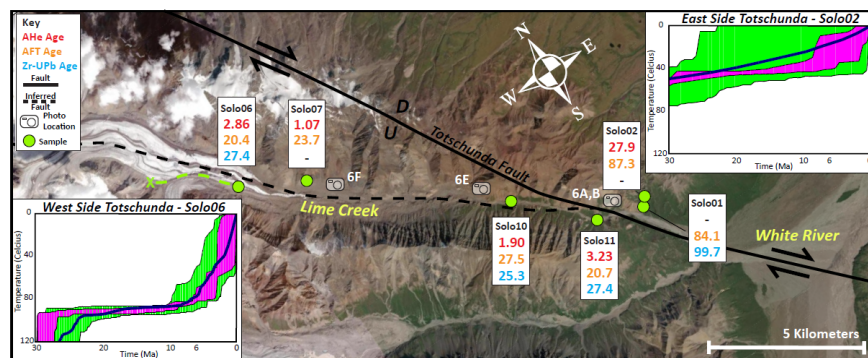


Figure 4: Compiled geochronology and thermochronology from Lime Creek Bedrock. AHe, AFT, and zircon U-Pb ages are displayed in colors coded in the key. Faults are denoted as solid lines or dotted where inferred. Small camera images and corresponding white letters denote image locations in Figure 6. For sample 19SOLO06, the dashed green line leading away from the sample location denotes inferred sample path for a

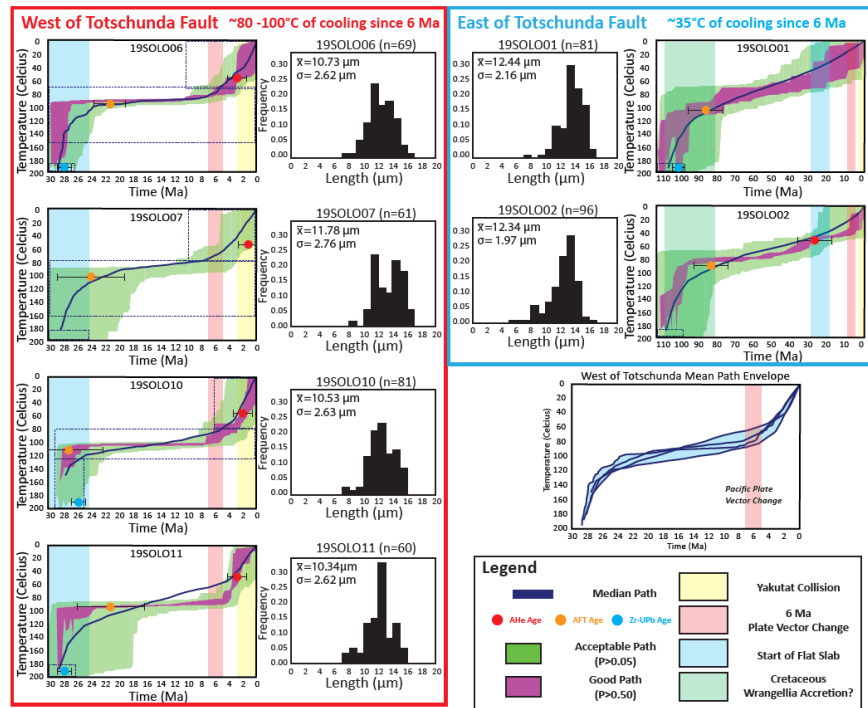
rock that clearly originated from the outcrop denoted with a green X. Representative thermal model for each side of the Totschunda fault shows that more recent rapid cooling occurred on the west side of the Totschunda fault than the east side of the structure.

4.1 LA-ICP-MS U-Pb Zircon Data

The U-Pb zircon ages for the hypabyssal bedrock in the Lime Creek drainage range from ca. 25 to 28 Ma (Table 1; S1, S2) and therefore these intrusions are associated with the Wrangell volcanic arc (Trop et al., 2022). The gabbro bedrock we sampled (19SOLO01 and 19SOLO02) was previously mapped as Triassic but our new data indicates this unit is Cretaceous in age (ca. 100 Ma). Gabbro units mapped as Triassic in the Lime creek area and within the McCarthy and Nabesna map areas (MacKevett, 1978; Richter, 1971) may warrant further inquiry to verify and better understand the spatial extent of Chisana arc Cretaceous aged magmatism (Manselle et al., 2020) in the region.

The cobbles we analyzed likewise have lithologies (porphyritic volcanics) and Oligocene-Miocene ages showing they too originated from Wrangell volcanic arc centers (e.g., Richter et al., 1990; Trop et al., 2022) (Figure 6; Tables 1, S1, S2). U-Pb ages for the felsic/intermediate detrital cobbles from the White River 'Tillites' are primarily from two populations: the first group consisting of three cobbles ranged in age from ca. 26 to 28 Ma and a second group consisting of four cobbles (from two locations) ranged in age from ca. 8.9 to 10 Ma (Figure 6).

4.2 Fission Track Data: bedrock samples and Late Miocene-Pleistocene detrital cobbles



Φηγυρε 5: ΗεΦΤψ μονελεδ 'γουδ-φητ' ανδ 'αρρεπαβλε-φητ' T-τ ενελοπερ φορ Οληγορνε ηηπαβηρροαλ ηντρυοε ρορκερ φρομ ηε ωεστ οηδε οφ ηε Τοτρρηνδα φαυλτ (λεφτ) ανδ ρεταρρεορ γαββροηρ ρορκερ φρομ ηε εαστ οηδε οφ ηε Τοτρρηνδα φαυλτ (ρηητ). ΑΗε, ΑΦΤ, ανδ ζηρροη Υ-Πβ αγερ αρε πλοττεδ οη ηε μονελερ ωηερε

απλισταβλε ωιτη 2σ error βαρς φορ ΑΗε ανδ Υ-Πβ δατες ανδ 1σ error βαρς φορ ΑΦΤ δατες. Τεστονις ανδ πλατε βουνδαρψ εεντς αρε λαβελεδ ας ζολορεδ σχυαρες ωιτη εξπλανατιον ιν τηε φηγυρε λεγεινδ. ορρεσπονδιγγ ΑΦΤ λεγγτη διστριβυτιονς αρε πλοττεδ το τηε ριγγητ ορ λεφτ οφ εαση σαμπλε. Τηε ‘μεαν’ ζοολιγγ πατη φορ αλλ τηε Ολιγοσενε ηψπαβψσσαλ ροσκς ις πρεσεντεδ ας α ζομποσιτε ζοολιγγ ενελοπε (σηων αρε μεδιαν πατης φορ αλλ ηψπαβψσσαλ σαμπλες). Ανωτοατεδ Υ-Πβ, ΑΦΤ, ανδ ΑΗε αγες ωερε νοτ υσεδ ας ζονοστραιντ βοξες δυριγγ ΗεΦΤψ μοδελιγγ.

Two bedrock samples (19SOLO01, 19SOLO02) from the Cretaceous gabbro immediately east of the Totschunda fault have AFT ages of 84 ± 8 Ma ($\pm 1\sigma$) (19SOLO01) and 87 ± 8 Ma (19SOLO02). Small plutonic bodies cool rapidly after emplacement (ca. <1 Ma) (Nabelek et al., 2012) so we infer these ages reflect exhumation related cooling and not post emplacement thermal relaxation given the ca. 100 Ma U-Pb zircon crystallization age of these gabbro samples.

On the west side of the Totschunda fault, four samples of Oligocene hypabyssal andesitic and dacitic porphyry plugs (19SOLO06, 07; 10; and 11) yield AFT ages of 20 ± 3 ($\pm 1\sigma$) (19SOLO06), 24 ± 5 (19SOLO07), 28 ± 5 (19SOLO10), and 21 ± 5 Ma (19SOLO11). The track length distributions of all six bedrock samples comprised a mix of long and shorter tracks indicative of complex thermal histories with significant residence time in a partial annealing zone (e.g., Gleadow et al., 1986) (Figure 5, Tables 2, S15).

The detrital cobble AFT ages can be divided into two groups: 30-35 Ma (19SOLO18 a, b, c) from three cobbles at one sample station and 8-13 Ma (19SOLO03 a, b, c and 19SOLO12 a, b) from five cobbles at two additional sample stations (Figures 3, 6; Tables 2, S16, S17). The uranium concentration in apatite crystals was low (4-7 pm) which resulted in relatively large uncertainties in AFT ages ($\pm 3-6$ Ma, $\pm 1\sigma$). Low [U] plus relatively young ages mean confined fission tracks suitable for track length measurement were rare. Without sufficient length measurements (> 25) we did not model these samples. However, AFT ages overlap within uncertainty of the U-Pb ages for the two groups (ca. 26 to 28 Ma and ca. 8.9 to 10 Ma; Figure 6). We interpret the cobble AFT data to indicate rapid cooling associated with post intrusion thermal relaxation of the original hypabyssal and volcanic units followed by exhumation, erosion, transportation and deposition in the basin.

4.3 Apatite and Zircon (U-Th)/He Data

We report inverse variance weighted mean AHe ages for five Lime Creek samples total (30 single-grain ages in total; Table 3 and Figures 4, 5, 6, S3-S6); one from the Cretaceous gabbro east of the Totschunda fault (single grain ages = 6; 53.4 - 9.0 Ma single grain ages) and four from Oligocene hypabyssal rocks west of the fault (single grain ages = 24; 4.7 - 0.5 Ma single grain ages). Single-grain AHe ages were not included in sample mean age calculations if they exceeded a z-score of two (two standard deviations from the overall sample population mean). For included single-grain age data, there was no strong correlation of [eU] vs. age or grain size (R_g) vs. age for any of these samples (see S6). The young AHe ages and low uranium concentrations in apatite from the Lime Creek drainage (~ 2.4 U pm for the hypabyssal intrusive rocks and ~ 4.7 U pm for the Cretaceous gabbro) reduced any possible radiation damage related kinetic effects (e.g., Flowers et al., 2009; Flowers et al., 2022a, b).

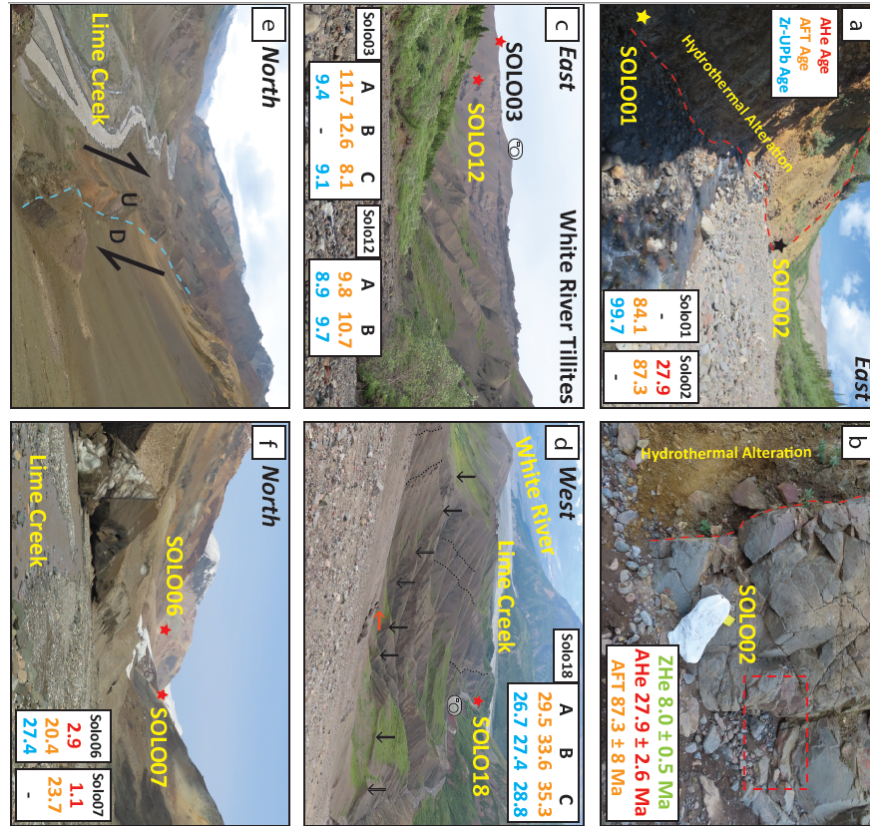


Figure 6: Photo Collage. Note that facing directions are given in black text at top of each figure where applicable. a) Sample location for 19SOLO02 showing heavily oxidized quasi-gossanous material downstream of the Cretaceous gabbro suggestive of local hydrothermal fluid flow. b) Sample location for 19SOLO02 showing where rocks were sampled (directly to the left of the bag) and heavily oxidized and weathered material to the left of the red line in the image. Red dashed square highlights hematite precipitation on fracture surfaces suggesting hydrothermal fluids at some point in the geologic past. ZHe, AFT, and AHe ages are displayed on the figure to document age ‘inversion’. c) Photo of the unnamed creek bed with the White River “Tillites” in the background. Small camera denotes location where photo 6D was taken, looking towards the location of this photo. Approximate cobble sample locations shown with sample name and red stars. d) Photo from ridge-top of White River ‘Tillites’ outcrop extent. Camera denotes image location of photo 6C that looks uphill towards this location. Red arrow denotes a geologist for scale. Black arrows highlight a Holocene (?) scarp on a splay of the Totschunda fault. Black dotted lines denote intersection of bedding planes with topography and approximate strike. Note the strong change in ‘strike’ of beds across the fault scarp. Lime Creek labeled in the background. e) Uptthrown fault blocks along the Totschunda fault in Lime Creek. Mapped fault trace continues out of frame along the creek and up through the mountainside. Fault blocks are dominantly comprised of Paleozoic metasediments and thus were not good targets for thermochronologic analyses but do make an impressive landscape feature. These upthrown blocks are probably $< \sim 25,000$ years old as otherwise they would have been removed by major glaciation in the valley (last glacial maximum; Kaufman et al., 2011). f) Sample locations for 19SOLO06 and 19SOLO07 shown as red stars. Lime Creek and Lime Glacier ice-cored moraine shown in the foreground.

ZHe dating was undertaken on the Cretaceous Gabbro to better resolve the thermal history of the rocks on the east side of the Totschunda fault (19SOLO02, Table 3; Figures 6, S3, S5, S6). 19SOLO02 single-grain ZHe ages from our analyses were the same regardless of [eU] or grain size. ZHe ages for sample 19SOLO02

yielded a mean age of 8.0 ± 0.5 Ma ($\pm 1\sigma$; single-grain ages = 3). This age is younger than both the AFT age (87.3 Ma) and the mean AHe age (27.9 Ma) although similar to the youngest AHe single-grain age (9 Ma) from this sample. High [eU] zircons dated using (U-Th)/He can have lower closure temperatures than apatite from the same sample due to radiation damage from high uranium concentrations facilitating diffusion of He from the grain (e.g., Johnson et al., 2017), but the [eU] for the three 19SOLO02 grains analyzed only ranges from ~ 100 to ~ 300 ppm (Table 3). However, sample 19SOLO02 was collected in an area of extensive penetrative fluid flow (approximately 200 meters wide) (Figures 6a, 6b). This 8.0 ± 0.5 Ma ZHe age from this sample is also similar in age to some of the ‘White River Tillites’ dated lava flows (8.4 ± 0.7 Ma; 8.7 ± 0.9 Ma; Denton and Armstrong, 1969) lying within the basin that is immediately adjacent to 19SOLO02 (Figure 3). We therefore infer the young ZHe age (relative to the AFT and AHe ages from the same sample 19SOLO02) of ca. 8 Ma is related to hydrothermal fluid flow along the Totschunda fault coeval with a dated magmatic event in the ‘White River Tillites’ area (Denton and Armstrong, 1969). Although the low [eU] zircons selected for (U-Th)/He dating had no evident cracks nor defects (S3), we suggest that He loss due to hydrothermal fluid flow in these zircons may be a physical process (such as leaching) and not exclusively due to volume diffusion (e.g., Johnson et al., 2017).

4.4 HeFTy Modeling

Multi-kinetic inverse thermal models for samples from the Cretaceous Gabbro and Oligocene porphyry samples were generated using HeFTy v. 1.9.3 (Ketcham, 2005; S7). Depicted constraint boxes were used in a later stage of modelling iterations to optimize the ratio between tried paths and good paths (S7). For the Cretaceous gabbro samples just east of the Totschunda fault (19SOLO01 & 19SOLO02; S8, S9) rapid cooling occurred around ca. 95 Ma to temperatures of $\sim 100^\circ\text{C}$ by ~ 85 Ma followed by very slow cooling ($\sim 0.8^\circ\text{C}/\text{Ma}$) to 60°C until ca. 25 Ma when more rapid cooling ($\sim 2.5^\circ\text{C}/\text{Ma}$) resumed (Figure 5). Overall, with little variation, the Oligocene hypabyssal porphyry plug samples (samples 19SOLO06; 07; 10 and 11; S10 - S13) preserve nearly identical thermal histories (Figure 5). Given the Oligocene crystallization ages for these magmatic bodies, we associate Oligocene rapid cooling with thermal relaxation after intrusion, followed by near isothermal shallow crustal residence until the Late Miocene when the hypabyssal rocks experienced rapid cooling due to inferred exhumation at $\sim 13^\circ\text{C}/\text{Ma}$ from ca. 6 Ma until present. The abrupt change in AHe ages across the Totschunda fault (ca. 28 Ma east side; ca. 2 Ma west side), the preserved upthrown blocks (Figures 4, 6) and the intrusive lithology of these Oligocene rocks support exhumation as the mechanism responsible for the recorded cooling.

5. Discussion

5.1 East Side of the Totschunda Fault Thermal Histories

The two samples of Cretaceous gabbro (19SOLO01 and 02) from the east side of the Totschunda fault document mid-Cretaceous (ca. ~ 95 Ma) cooling of $\sim 5^\circ\text{C}/\text{Ma}$, then ca. 70 million years of relatively slow cooling ($< 1^\circ\text{C}/\text{Ma}$) followed by an increase in cooling rate to $\sim 2.5^\circ\text{C}/\text{Ma}$ in the Late Miocene. Given that the U-Pb zircon emplacement age is ca. 100 Ma (19SOLO01), and AFT ages are 84-87 Ma, we infer that Cretaceous cooling is due to regional exhumation, consistent with similar Cretaceous cooling ages observed west of the central Totschunda fault by Milde (2014). We acknowledge that track shortening from long residence times in the PAZ would have reduced the fission track age, but given the coarse-grained nature of the intrusive rock implying emplacement below the PAZ (~ 5 km) we think Cretaceous exhumation is more apt. These gabbroic rock samples then slowly cooled or were near isothermal from the mid-Late Cretaceous until the Late Miocene where a small pulse of more rapid cooling is evident ($\sim 35^\circ\text{C}$ since 6 Ma). This Late Miocene cooling is significantly less than the observed Late Miocene-Present cooling on the west side of the Totschunda fault ($\sim 100^\circ\text{C}$ since 6 Ma).

5.2 West side of the Totschunda fault Thermal Histories

U-Pb zircon ages from hypabyssal rocks on the west side of Totschunda fault (samples 19SOLO06; 07; 10 and 11) yield Oligocene ages. Thus, these rocks only constrain post-Oligocene tectonic activity along the Totschunda fault, but we infer their emplacement is related to concurrent transtensional magmatism along the fault (e.g., Blanquat et al., 1998). Given the partial overlap of the AFT ages with U-Pb zircon ages for the hypabyssal samples west of the Totschunda fault (25-28 Ma) and the complex track length distributions, we interpret these rocks to have been emplaced at relatively shallow depths in concurrence with their lithology, followed by residence in the partial annealing zone before later cooling and inferred exhumation. The overlap in fission track and U-Pb zircon ages therefore reflects the timing of crystallization. However, the paucity of longer tracks relative to shorter more-annealed tracks in the Oligocene hypabyssal rocks suggests these rocks were exhumed in the recent geologic past (Figure 5). The HeFTy thermal models further constrain this history with residence in a partial annealing zone from the time of emplacement until ~6 Ma when they were rapidly cooled. The AHe ages (3.23 - 1.07 Ma) also indicate continued rapid cooling through the Pliocene and into the Pleistocene. We interpret this Late Miocene cooling as related to rejuvenated horizontal slip and associated exhumation along the Totschunda Fault.

5.3 The case against thermal perturbation for our samples

The case for thermal perturbation resulting from nearby magmatism (or resultant hydrothermal effects) in our samples is generally poor except for the ZHe results from sample 19SOLO02 as discussed above. While young Wrangell arc lavas nearby have similar Late Miocene - recent ages of eruption compared to AHe ages from the hypabyssal samples (Denton and Armstrong, 1969; Richter et al., 1990; Trop et al., 2022), the fact that the gabbro sample from east of the Totschunda Fault preserves an AHe age that is much older than the nearby lavas (<1 km distance, 27 Ma AHe age vs 2 Ma age of lava) suggests that these lavas did not reset the AHe system in our hypabyssal intrusive rocks. The young AHe ages in our hypabyssal rocks therefore reflect exhumation related cooling. The hypabyssal rocks themselves hypothetically could have reset the AHe ages for the Cretaceous aged gabbro, as the AHe gabbro age (ca. 27 Ma) is the similar as the intrusive ages of the hypabyssal rocks that are only 1.5 km away (25-28 Ma). However, the overall large spread in single grain AHe ages (53.4-9.0 Ma) from the gabbro imply the sample did not experience a significant heating-cooling event at ca. 27 Ma.

5.4 Climatic Forcing of Rock Cooling (?)

The Pleistocene AHe ages from the southern Totschunda fault overlap with the timing of Northern Hemisphere glaciations (e.g., Raymo, 1994). Some researchers have suggested that glaciation can lead to periods of rapid erosion, and thus, rapid exhumation (e.g., Spotila et al., 2004; Huntington et al., 2006; Blythe et al., 2017). If some of the sediments in the White River 'Tillites' have a glacial origin, increased climate forcing (i.e., glaciation) could, in part, be responsible for the recorded exhumation. If true, one should expect Pleistocene AHe ages everywhere there was glaciation in the Lime Creek drainage with the youngest cooling ages at the lowest elevations regardless of structural position (i.e., proximity to the fault). That is not the case as shown by the Oligocene AHe ages from Cretaceous gabbro samples collected ~35 m above the valley floor that have ages of ca. 27 Ma as compared to two samples collected ~400 m above the valley floor, that have younger Plio-Pleistocene AHe cooling ages (Figure 6). Additionally, the Totschunda fault is in the rain shadow of the Saint Elias Range and considered an area where surface processes' control on cooling age patterns are limited during the late Cenozoic (Enkelmann et al., 2017). Overall, the pattern of thermochronologic ages show a structural control-contrasting ages across the Totschunda fault (ages are younger to the west, older to the east) indicative of west-side up displacement. This pattern of younger thermochronologic ages to the west of the fault was also recognized by Milde (2014) on the central Totschunda fault.

5.5 Detrital Cobbles and the White River ‘Tillites’

The different zircon U-Pb and AFT age populations between the two groups of porphyritic andesite and dacite cobbles collected from different stratigraphic positions may reflect a change in provenance during deposition of basin sediments; however the stratigraphic ages of the cobbles are poorly constrained given the deformational history of the basin (Denton and Armstrong, 1969; Eyles and Eyles, 1986). The K-Ar ages on lavas within the stratigraphic section reported by Denton and Armstrong (1969) constrain the timing of sedimentation but given post-depositional deformation are insufficient to resolve the stratigraphic position of the cobbles. Regardless, the cobbles were deposited at the surface sometime between ca. 10 and 2 Ma.

At one outcrop near the base of the section, sample 19SOLO18B has a mean track length of 10.8 mm (n=12) and sample 19SOLO18C from the same location has a mean track length of 14.6 mm (n=15). Overlapping U-Pb and AFT ages for this stratigraphically lowermost outcrop indicate that both clasts originate from coeval subvolcanic or volcanic rocks and both clasts shared the same depositional history. Cobble 19SOLO18C, with little track shortening, had to come from a rock emplaced above the PAZ or erupted on the surface (cooler than 60°C) and never buried to higher temperatures. Significant track shortening in Cobble 19SOLO18B suggests residence in the PAZ, which could potentially have occurred either before source rock exhumation (as in the bedrock samples analyzed) or in the basin during burial. This latter option is unlikely as both cobbles 19SOLO18B and 19SOLO18C must share the same depositional history. Therefore, our cobble AFT data do not record the burial nor exhumation history of this “thin” sedimentary basin. Instead, the cobbles document that there has been little to no thermal resetting in the tillite strata. We therefore cannot constrain the timing of basin deformation and unroofing using the AFT data. Unlike thicker foreland basins where the AFT cobble thermochronology method works well (Beamud et al., 2011; Fitzgerald et al., 2019), we suggest that application of this method to constrain the timing of basin inversion in smaller relatively short-lived basins formed along strike-slip faults is unlikely to work in many cases due to insufficient burial (~3-5 kms) to fully or partially reset the AFT system.

5.6 Tectonic Significance

5.6.1 Mid-Cretaceous to Late Miocene

The two mid-Cretaceous gabbroic samples from east of the Totschunda fault preserve Late Cretaceous cooling which may be related to Mesozoic slip along the Totschunda fault. The thermal history after ca. 85 Ma for our gabbroic rocks on the east side of the Totschunda fault shows prolonged slow cooling until the Late Miocene.

While we observe no pulses of Oligocene rapid cooling in any of our samples, available geologic evidence suggests the Totschunda fault has been continuously active since the Oligocene. The available geologic evidence is as follows: 1) Oligocene-Miocene thrust-top basins along the Totschunda fault after palinspastic reconstruction (Allen et al., 2018); 2) Rapid Oligocene cooling in Cretaceous aged intrusive rocks along the central segments of the Totschunda fault (Milde, 2014); 3) Diking into the central Totschunda fault zone from ca. 29 Ma to 23 Ma linked with fault zone fluid flow and transtension (Brueseke et al., 2019); 4) Magmatism in the Sonya Creek Volcanic field ca. 23 to 19 Ma associated with transtension along the Totschunda fault (Berkelhammer et al., 2019); and 5) Oligocene-early Miocene Wrangell Arc magmatism along the Totschunda fault (Trop et al., 2022, this study).

Therefore, we conclude that the Totschunda fault experienced strike-slip motion ca. 25 to ca. 6 Ma, though at much reduced rates (~2 mm/yr) compared to ca. 6 Ma to modern rates (~14 mm/yr; Marechal et al., 2018; Allen et al., 2022). This slip-rate calculation of ~2 mm/yr is based on 1) ~125 km allowable Totschunda fault slip since 52 Ma (Clearwater-Talkeetna fault to Nutzotin-Totschunda fault offset), and 2) the estimated ~85 km of Totschunda fault slip since 6 Ma (Berkelhammer et al., 2019; Waldien et al., 2021; Allen et al., 2022) (Figures 1, 7). This leaves 40 km of required slip over ~20 million years equating to 2 mm/yr.

5.6.2 Late Miocene - Present: Eastern Denali-Totschunda Fault Reorganization

In the past 20 million years, the most significant plate boundary events along the Alaska southern margin are the following:

The ca. 6 Ma Pacific-Yakutat plate vector change and associated 37% net increase in convergence rate between the Pacific and North American plates (e.g., Engebretsen, 1985; Doubrovine and Tarduno, 2008; Austerman et al., 2011) and

Following 29 million years of the Yakutat flat slab subduction, final collision of the eastern Yakutat ~30 km thick oceanic plateau segment at ca. 1 Ma (e.g., Richter et al., 1990; Gulick et al., 2013; Brueseke et al., 2023).

These tectonic events have reshaped the Alaska plate boundary and the faults which accommodate stresses transferred inboard from this convergent margin.

Numerous authors have referred to the ‘collision’ of the Yakutat oceanic plateau starting as early as the Oligocene and Mio-Pliocene (Chapman et al., 2008; Enkelmann et al., 2010; Lease et al., 2016) and as late as 1 Ma (e.g., Reece et al., 2013; Brueseke et al., 2023). Here, we define collision as the cessation of Wrangell arc magmatism and the abandonment of the subduction zone trench (e.g., McGeary et al., 1985). Evidence against a 6 Ma Yakutat ‘collision’ event are the following: 1) Based on migrating patterns of arc magmatism, the subducting Yakutat slab apparently accelerated in subduction rate (or flattened, but continued subducting) between 6 Ma and 1 Ma (Richter et al., 1990; Trop et al., 2022); 2) The Wrangell arc was still robustly active between 6 Ma and 1 Ma (Richter et al., 1990; Trop et al., 2022); and 3) The now colliding 30 km thick segment of the Yakutat terrane (Worthington et al., 2012) would have been roughly 300 km outboard of the North American margin ~ 6 million years ago based on modern Pacific-Yakutat plate/North America ~50 km/Ma convergence rates (Elliot et al., 2010).

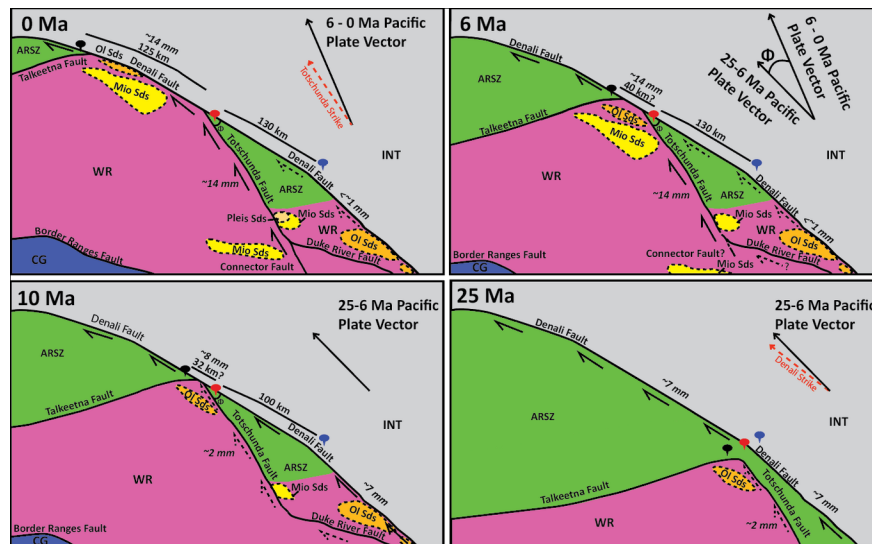


Figure 7: Schematic palinspastic reconstructions of strike-slip translation and basin formation in eastern Alaska and the Yukon from 25 Ma to present. Pacific- Yakutat microplate vectors through time (Doubrovine and Tarduno, 2008; Elliot et al., 2010; Elliott and Freymuller 2020) and strike of Eastern Denali fault and Totschunda fault shown in upper right corner of figures when applicable. Major faults and geologic units are labeled in each figure. Blue pin is arbitrary and fixed relative to the red and black pins. Blue-red pins demonstrate 130 km of right-lateral slip on the Eastern Denali fault from 25 Ma to 6 Ma using long term slip rates of ~7mm/yr. (Waldien et al., 2018) for the given time period. Black-red pins demonstrate ~40 km

of allowable right-lateral slip on the Totschunda fault from 25 Ma to 6 Ma (~ 2 mm/yr) and an additional 85 km of right-lateral slip on the Totschunda fault from 6 Ma to present (14 mm/yr) using long term slip rates and total separation between the correlative Nutzotin basin sediments (Red Pin) and Clearwater sediments (Black Pin) (Waldien et al., 2018; Berkelhammer et al., 2019; Allen et al., 2022). Strike-slip motion is minimal if at all along the northern Eastern Denali fault after ca. 6 Ma (e.g., Marechal et al., 2018; Choi et al., 2021). WR - Wrangellia; ARSZ - Alaska Range Suture Zone; CG-Chugach Terrane; INT-Intermontane Terrane / North America; Ol Sds-Oligocene Sediments; Mio Sds-Miocene Sediments; Pleis Sds-Pleistocene Sediments.

Our new thermochronology data documents an increase in cooling, inferred exhumation, and slip rates at 6 Ma along the Totschunda fault. We conclude the ca. 6 Ma Pacific-Yakutat plate vector change (Engebretson et al., 1985) was responsible for transferring slip away from the northern Eastern Denali fault and onto the Totschunda fault at this time. The ca. 1 Ma collision of the ~ 30 km thick Yakutat segment and subsequent jamming of the Wrangell arc trench (Richter et al., 1990; Christenson et al., 2012; Gulick et al., 2013; Reece et al., 2013; Trop et al., 2022; Brueseke et al., 2023) may have further accelerated stress transfer from the plate boundary along the Fairweather transform to the Totschunda fault via the inferred Connector fault (e.g., Richter et al., 1971; Lahr and Plafker, 1980; Spotila and Berger 2010; Doser, 2014).

The Late Miocene (ca. 6 Ma) southern Alaska tectonic event documented by numerous previous thermochronology studies across and along the Denali fault system (e.g., Fitzgerald et al., 1993, 1995; Waldien et al., 2018; Benowitz et al., 2022a, b) has been linked to the Pacific-Yakutat plate vector change at ca. 6 Ma. This event led to a profound change in slip distribution on faults across southern Alaska. Rocks along other fault systems such as the Fairweather fault corridor (McAleer et al., 2009), Queen Charlotte fault zone (Cromwell, 2021), St. Elias Range (Enkelmann et al., 2017); western Chugach mountains (Arkle et al., 2013); as well as the Tordrillo Mountains (Haeussler et al., 2008) all experienced a pronounced increase in exhumation at ca. 6 Ma. Additional studies document increases in the progression of magmatism in the Wrangell volcanic field ca. 6 Ma (Richter et al., 1990; Trop et al., 2022), initiation of the magmatism on the Seward Peninsula (Mukasa et al., 2007), rejuvenation of the Aleutian island arc (Jicha et al., 2006), extension in the Bering Sea (Marincovich et al., 1999), formation of the Mount McKinley restraining bend (Benowitz et al., 2022b) and coarse clastic sedimentation rates along the Denali fault and Cook Inlet increasing in the Late Miocene (Wahraftig, 1975; Ridgway et al., 2007; Finzel et al., 2015; Allen et al., 2022) (Figure 8).

Furthermore, the increase in deformation along the west side of the Fairweather fault related to the ca. 6 Ma Pacific-Yakutat plate vector change (McAleer et al., 2009) resulted in a “double-trouble” tectonic scenario along the St. Elias syntax. The continued flat slab-subduction of the Yakutat oceanic plateau combined with convergence of the crustal welt along the western Fairweather fault led to increased deformation along the St. Elias coastal mountains (Enkelmann et al., 2010). However, there is no evidence the indentation of the Fairweather Fault sliver led to increased slip rates on the Totschunda fault since 6 Ma.

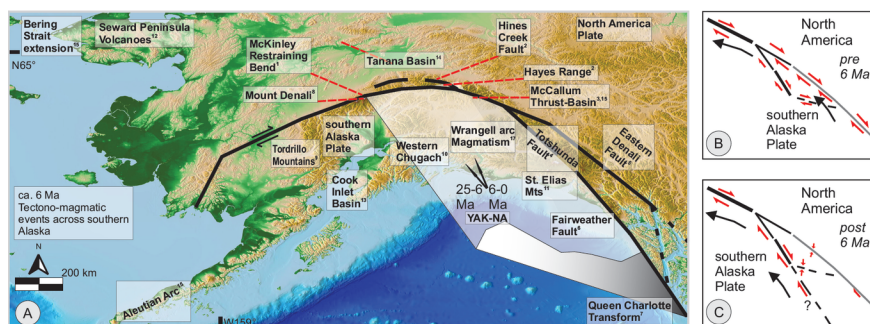


Figure 8: a) Compilation of the location tectonic and magmatic events across southern Alaska that occurred in response to the ca. 6 Ma Pacific plate motion change. Yakutat slab position at ca. 6 Ma is inferred

based on restored modern ~ 50 mm/yr slab slip rates and does not include ~ 1000 km of likely eclogitized slab by that time (Rossi et al., 2006). References: fault modification:¹Benowitz et al. (2022a); ²Benowitz et al. (2022b); ³Waldien et al. (2018);⁴this study, ⁵Choi et al. (2021);⁶McAleer et al. (2009); ⁷Hyndman (2015). Orogenesis increase: ⁸Fitzgerald et al. (1993, 1995); ²Benowitz et al. (2022b);⁹Haeussler et al. (2008); ¹⁰Arkle et al. (2013); ¹¹Enkelmann et al. (2017). Basin evolution: ¹²Marincovich and Gladenkov (1999);¹³Finzel et al. (2015); ¹⁴Ridgway et al. (2007); ¹⁵Allen et al. (2022). Magmatism change:¹⁶Mukasa et al. (2007); ¹⁷Richter et al. (1990). Also see text for additional references for these ca. 6 Ma southern Alaska tectono-magmatic events. Base layer from Lim et al. (2011). b) and c) Schematic of pre and post ca. 6 Ma slip distribution and block motion along the Totschunda and eastern Denali faults. Before ca. 6 Ma the Totschunda and Duke River faults were translated along the curve of the Denali fault leading to variable orientations in relation to relative Pacific plate convergence direction. Modified from Marechal et al. (2018).

Lastly, the Totschunda fault strikes 326° , the northern Eastern Denali fault has a general strike of 308° , while the incoming Yakutat microplate is converging at 337° relative to southeastern Alaska (Elliott et al., 2010). The strike of these faults and when they are active is correlative with the relative convergence direction of the subducting plate. The change in relative plate motion and $\sim 37\%$ increase in net convergence rate in the Late Miocene (ca. 6 Ma) to a more northerly orientation is better aligned with the strike of the Totschunda fault versus the strike of the Eastern Denali fault. This Late Miocene event correlates with the inferred change in slip distribution from 7 mm/yr of horizontal motion on the Eastern Denali fault and <2 mm/yr on the Totschunda fault to <1 mm/yr on the Eastern Denali fault and 14 mm/yr on the Totschunda fault (Figure 7). We suggest that the strike of the Totschunda fault was more favorably aligned than the Eastern Denali Fault to accommodate slip following the Late Miocene relative plate motion change since the Totschunda fault is nearly parallel to the plate vector of the Pacific-Yakutat plate. Conversely, prior to the Late Miocene the Eastern Denali fault was nearly parallel to the plate motion vector of the then slower moving Pacific-Yakutat plate. Thus, the fault system has changed from the Central Denali fault receiving slip from the Eastern Denali fault to the Central Denali fault receiving slip from the Totschunda fault (Figure 7).

In summary the newly presented thermochronologic constraints from the Totschunda fault in conjunction with: 1) The general absence of younger-than-Late Miocene rapid exhumation on the northern Eastern Denali fault (e.g., McDermott et al., 2019) (Figure 2a); 2) The Eastern Denali fault acting as a backstop with little to no dextral slip component since the Late Miocene (e.g., Enkelmann et al., 2022), 3) Limited to no Holocene strike-slip motion on the modern Eastern Denali fault (Marechal et al., 2018), and 4) Seismic analysis indicating the Eastern Denali fault is not presently an active strike-slip fault due to unfavorable perpendicular principal stresses (Choi et al., 2021) supports that the ca. 6 Ma Pacific-Yakutat plate vector change redistributed almost all horizontal slip from the Eastern Denali fault onto the Totschunda fault. Hence, we concur with numerous other studies that suggest a less active (“sleepy”) northern Eastern Denali fault after ca. 6 Ma (Waldien et al., 2018; Choi et al., 2021; Trop et al., 2022; Allen et al., 2022). An increase in exhumation rates in the central Alaska Range (Fitzgerald et al., 1993, 1995), the development of the Mount McKinley restraining bend (Benowitz et al., 2022b), expansion of the Alaska Range Northern foothills fold and thrust belt and Hayes Range deformation front (Bemis et al., 2015, Benowitz et al., 2022a); and exhumation in the Tordrillo Mountains (Haeussler et al., 2008) are all in part a deformational response to this Late Miocene plate boundary modification.

5.7 Global Context

Around the Pacific plate, convergence was either redistributed along preferentially aligned pre-existing faults or fault systems were modified to accommodate a change in incoming strain direction following the ca. 6 Ma Pacific plate motion change. This is observed on the Denali fault: (Fitzgerald et al., 1993, 1995; Benowitz et al., 2022a, b); the Totschunda fault (this study), the Queen Charlotte fault (Hyndman, 2015); the San Andreas fault (Kellogg and Minor, 2005; Townsend et al., 2021), the La Cruz fault (Bennett et al., 2016), and the Alpine fault system of New Zealand (Walcott 1998; Batt et al., 2004; Collett et al., 2019; Duvall et al., 2020). This change in relative plate motion in the Late Miocene (ca. 6 Ma) resulted in geodynamic responses

that were near geologically instantaneous. Hence, these slip redistribution events support the theorem that deformation seeks the path of least resistance or work minimalization, such that the “*Earth is lazy*” (Cooke and Madden, 2014) and fault systems evolve towards mechanical efficiency both through time and space to accommodate new stress regimes. As fault intersections are common along strike-slip fault systems (e.g., San Jacinto-San Andreas faults), fault strike obliquity relative to incoming plate vectors can be used, with caution for seismic hazard prediction (Schwartz et al., 2012; Lozos, 2016) and to evaluate which fault is the strand of principal slip (Christie-Blick and Biddle, 1985; Passchier and Platt, 2017).

6. Conclusions

By integrating our new geochronology and thermochronology data from the southern part of the Totschunda fault with a compilation of geologic data from across southern Alaska we increased our understanding of the Totschunda-Denali fault system and southern Alaska tectonics. The key findings are:

1. Inverse thermal models (HeFTy) of apatite Fission track, (U-Th)/He, and U-Pb indicate a rapid exhumation event ($\sim 13^\circ\text{C}/\text{Ma}$) initiated on the southern segment of the Totschunda fault at ca. 6 Ma.
2. We suggest slip rates of ~ 2 mm/yr on the Totschunda fault from ca. 25 Ma to 6 Ma to accommodate ~ 40 km of dextral displacement.
3. Starting in the Late Miocene (~ 6 Ma) slip rates on the Totschunda fault accelerated from ~ 2 mm/yr to ~ 14 mm/yr as strain from the southern Alaska margin was accommodated by the Totschunda fault while the northern Eastern Denali fault was effectively abandoned. This change is a result of a relative plate motion change between the Pacific-Yakutat plates and North America.
4. We suggest that circum-Pacific Plate fault reorganizations were compelled by the ca. 6 Ma Pacific plate motion change with the nature for slip along fault systems to be redistribution towards mechanical efficiency (Cooke and Madden, 2014; McBeck et al., 2017).

Ancillary findings from the study area include 1) Cretaceous rapid cooling from ~ 95 Ma to ~ 85 Ma ($\sim 10^\circ/\text{Ma}$) is documented on a small Cretaceous gabbro unit, 2) U-Pb zircon ages document Oligocene Wrangell Arc volcanism along the Totschunda fault and refine a previously mapped “Triassic gabbro” as Cretaceous in age and 3) we suggest many basins formed along strike-slip faults are likely to be poor targets to apply cobble thermochronology in order to constrain the timing of basin inversion because of their relatively short-lived nature and small size.

7. Acknowledgements

We acknowledge support from National Science Foundation Tectonics Grant EAR-1550034 for fieldwork and analytical costs (to Fitzgerald) and Grant EAR-1550123 (to Benowitz) and from Syracuse University (Prucha and Nelson funds). This manuscript benefited from thorough and constructive reviews by Mauricio Parra and Terry Pavlis. We thank Dustin Trail and Amanda Maslyn at the University of Rochester for their assistance in generating the U-Pb zircon data.

8. Data Availability Statement

All data supporting the interpretations and conclusions of this study are in the manuscript text, figures, and the supplementary files (Mendeley Data, V1, DOI: 10.17632/pwctg84sxm.1). Field notes, lab notes, and samples are available upon request from the authors.

Tables:

Table 1: U-Pb Zircon Data

Uranium Lead Data

Sample

Sample	Type	Latitude (°N)	Longitude (°E)	Elev. (m)	No. of Grains	Fission Track Den- sity Rho- D (x 10 ⁶ cm ⁻²)	Fission Track Den- sity Rho- S (x 10 ⁶ cm ⁻²)	Fission Track Den- sity Rho- I (x 10 ⁶ cm ⁻²)	Fission Track Den- sity Ns	Fission Track Den- sity Ni	Fission Track Den- sity II(χ ²)	U (ppm)	Age (Ma)	Uncertainty (± 1)	Disc. (%)
19SOLOB1	Bedrock	61.763	-	1330	25	0.974	0.343	0.719	265	556	1.0	9.1	84.1	8.1	0
				141.832											
19SOLOB2	Bedrock	61.762	-	1341	25	0.994	0.318	0.644	302	611	1.0	8.1	87.3	8.1	0
				141.834											
19SOLOB3	Bas	61.783	-	1752	26	1.004	0.039	0.458	17	199	0.4	5.7	11.7	4.4	65
				141.829											
19SOLOB4	Bas	61.783	-	1752	30	1.014	0.039	0.475	30	366	0.9	5.9	12.6	3	0
				141.829											
19SOLOB5	Bas	61.783	-	1752	24	1.033	0.023	0.538	7	162	0.4	6.7	8.1	3.3	49
				141.829											
19SOLOB6	Bedrock	61.831	-	1981	30	1.053	0.056	0.512	78	714	1.0	6.2	20.4	2.7	0
				142.032											
19SOLOB7	Bedrock	61.820	-	1798	25	1.083	0.038	0.313	28	229	1.0	3.6	23.7	4.9	0
				141.996											

19SOLOC	B0	Bedrock	61.784	-	1402	25	1.276	0.030	0.250	37	306	1.0	2.1	27.5	5	0
			141.899													
19SOLOC	B1	Bedrock	61.766	-	1325	25	1.136	0.028	0.270	18	175	1.0	3.0	20.7	5.3	0
			141.862													
19SOLOC	C1a	Clst	61.778	-	1600	30	1.159	0.031	0.492	23	367	0.7	5.4	9.8	2.9	0
			141.830													
19SOLOC	C1b	Clst	61.778	-	1600	29	1.171	0.026	0.439	11	183	0.6	4.7	10.7	4.1	46
			141.830													
19SOLOC	C1a	Clst	61.763	-	1333	37	1.240	0.090	0.674	84	627	1.0	6.8	29.5	3.8	0
			141.834													
19SOLOC	C1b	Clst	61.763	-	1333	35	1.251	0.120	0.763	121	771	1.0	7.8	33.6	3.9	0
			141.834													
19SOLOC	C1c	Clst	61.763	-	1333	26	1.275	0.109	0.679	59	368	1.0	6.7	35.3	5.5	0
			141.834													

WGS
84

Elev.																
El-																
e-																
va-																
tion																
in																
me-																
ters;																
Stan-																
dard																
mea-																
sured																
flu-																
ence																
from																
stan-																
dard																
glasses;																
Rho-																
S –	S –	S –	S –	S –	S –	S –	S –	S –	S –	S –	S –	S –	S –	S –	S –	S –
den-																
sity																
of																
spon-																
ta-																
neous																
fis-																
sion																
tracks;																
Rho-																
I –	I –	I –	I –	I –	I –	I –	I –	I –	I –	I –	I –	I –	I –	I –	I –	I –
den-																
sity																
in-																
duced																
fis-																
sion																
tracks;																
n –	n –	n –	n –	n –	n –	n –	n –	n –	n –	n –	n –	n –	n –	n –	n –	n –
num-																
ber																
of																
track																
lengths;																
$P(\chi^2)$																
Chi																
squared																
value;																
U	U	U	U	U	U	U	U	U	U	U	U	U	U	U	U	U
ura-																
nium																
con-																
cen-																
tra-																
tion;																
SD																

Table 2: Summary of Apatite Fission track data (see supplementary data for details).

Table 3: (U-Th)/He Data

(U - Th)/ He Data

Sample Name and aliquot^a

_A01

_A02

_A03

_A04

_A05

_A06

_Z01

_Z02

_Z03

References

- Allam, A. A., Schulte-Pelkum, V., Ben-Zion, Y., Tape, C., Rupert, N., and Ross, Z. E. (2017). Ten-kilometer vertical Moho offset and shallow velocity contrast along the Denali fault zone from double-difference tomography, receiver functions, and fault zone head waves: *Tectonophysics*, v. 721, p. 56-69.
- Allen, W. K., Ridgway, K. D., Benowitz, J. A., Waldien, T. S., Roeske, S. M., Fitzgerald, P. G. and Gillis, R. J. (2022). Neogene sedimentary record of the evolution of a translated strike-slip basin along the Denali fault system: Implications for timing of displacement, composite basin development, and regional tectonics of southern Alaska. *Geosphere*, 18(2), p. 585-615.
- Arkle, J. C., Armstrong, P. A., Haeussler, P. J., Prior, M. G., Hartman, S., Sendziak, K. L. and Brush, J. A. (2013). Focused exhumation in the syntaxis of the western Chugach Mountains and Prince William Sound, Alaska. *Bulletin*, 125(5-6), p. 776-793.
- Austermann, J., Bird P., Heidbach O., Schubert G., and Stock J. M. (2011). Quantifying the forces needed for the rapid change of Pacific plate motion at 6 Ma. *Earth and Planetary Science Letters* 307, no. 3-4, p. 289-297.
- Barth, N. C., Boulton, C., Carpenter, B. M., Batt, G. E., and Toy, V. G. (2013). Slip localization on the southern Alpine fault, New Zealand: *Tectonics*, v. 32, p. 620-640.
- Bankey, V., Cuevas, A., Daniels, D., Finn, C. A., Hernandez, I., Hill, P., Kucks, R., Miles, W., Pilkington, M., Roberts, C., Roest, W., Rystrom, V., Shearer, S., Snyder, S., Sweeney, R. E., Velez, J., Phillips, J. D., Ravat, D. K. A. (2002). Digital data grids for the magnetic anomaly map of North America: U.S. Geological Survey Open-File Report 2002-414
- Batt, G. E., Baldwin, S. L., Cottam, M. A., Fitzgerald, P. G., Brandon, M. T., & Spell, T. L. (2004). Cenozoic plate boundary evolution in the South Island of New Zealand: New thermochronological constraints. *Tectonics*, 23 (4).
- Beamud, E, Muñoz, J. A., Fitzgerald, P. G., Baldwin, S. L., Garcés, M., Cabrera, L., Metcalf J. R. (2011). Magnetostratigraphy and detrital apatite fission track thermochronology in syntectonic conglomerates: constraints on the exhumation of the South-Central Pyrenees. *Basin Res* 23, p. 309-331.
- Bemis, S. P., Weldon, R. J., and Carver, G. A. (2015). Slip partitioning along a continuously curved fault: Quaternary geologic controls on Denali fault system slip partitioning, growth of the Alaska Range, and the tectonics of south-central Alaska: *Lithosphere*, v. 7, no. 3, p. 235-246.
- Bennett, S. E., Oskin, M. E., Iriondo, A. and Kunk, M. J. (2016). Slip history of the La Cruz fault: Development of a late Miocene transform in response to increased rift obliquity in the northern Gulf of California. *Tectonophysics*, 693, p. 409-435.
- Benowitz, J. A., Roeske, S. M., Regan, S. P., Waldien, T. S., Elliott, J. L. and O'Sullivan, P. B. (2022a). Large-scale, crustal-block vertical extrusion between the Hines Creek and Denali faults coeval with slip localization on the Denali fault since ca. 45 Ma, Hayes Range, Alaska, USA. *Geosphere*.
- Benowitz, J. A., Layer, P. W. and Vanlaningham, S. (2014). Persistent long-term (c. 24 Ma) exhumation in the Eastern Alaska Range constrained by stacked thermochronology. *Geological Society, London, Special Publications*, 378(1), p.225-243.
- Benowitz, J. A., Haeussler, P. J., Layer, P. W., O'Sullivan, P. B., Wallace, W. K. and Gillis, R. J. (2012). Cenozoic tectono-thermal history of the Tordrillo Mountains, Alaska: Paleocene-Eocene ridge subduction, decreasing relief, and late Neogene faulting. *Geochemistry, Geophysics, Geosystems*, 13(4).

- Benowitz, J. A., Davis, K. and Roeske, S. (2019). A river runs through it both ways across time: $^{40}\text{Ar}/^{39}\text{Ar}$ detrital and bedrock muscovite geochronology constraints on the Neogene paleodrainage history of the Nenana River system, Alaska Range. *Geosphere*, 15(3), p. 682-701.
- Benowitz, J.A., Layer, P. W., Armstrong, P., Perry, S.E., Haeussler, P.J., Fitzgerald, P.G. and VanLaningham, S. (2011). Spatial variations in focused exhumation along a continental-scale strike-slip fault: The Denali fault of the eastern Alaska Range. *Geosphere*, 7(2), p. 455-467.
- Berkelhammer, S. E., Brueseke, M.E., Benowitz, J.A., Trop, J.M., Davis, K., Layer, P.W. and Weber, M. (2019). Geochemical and geochronological records of tectonic changes along a flat-slab arc-transform junction: Circa 30 Ma to ca. 19 Ma Sonya Creek volcanic field, Wrangell Arc, Alaska. *Geosphere*, 15(5), p.1508-1538.
- Berger, A., Egli, D., Glotzbach, C., Valla, P.G., Pettke, T., Herwegh, M. (2022). Apatite low temperature chronometry and microstructures across a hydrothermally active fault zone, *Chemical Geology* 588
- Betka, P.M., Gillis, R.J., and Benowitz, J.A., Cenozoic sinistral transpression and polyphase slip within the Bruin Bay fault system, Iniskin-Tuxedni region, Cook Inlet, Alaska: *Geosphere*, v. 13, no. 6, p. 1806-1833, doi:10.1130/GES01464.1.
- Black, L.P., Kamo, S.L., Allen, C.M., Davis, D.W., Aleinikoff, J.N., Valley, J.W., Mundil, R., Campbell, I.H., Korsch, R.J., Williams, I.S., Foudoulis, C. (2004). Improved $^{206}\text{Pb}/^{238}\text{U}$ microprobe geochronology by the monitoring of a trace-element-related matrix effect; SHRIMP, ID-TIMS, ELA-ICP-MS and oxygen isotope documentation for a series of zircon standards, *Chemical Geology*, Volume 205, Issues 1-2, 2004, p. 115-140.
- Blanquat, M. D. S., Tikoff, B., Teyssier, C., Virgneresse, J.L. (1998). Transpressional kinematics and magmatic arcs, In: Holdsworth, R. E., Strachan, R. A., Dewzy, J. E (eds) (1998). *Continental Transpressional and Transtensional Tectonics*. Geological Society, London, Special Publications, 135, p. 327-340.
- Blythe, A. E., House, M. A., Spotila, J. A. and Barth, A. (2002). Low temperature thermochronology of the San Gabriel and San Bernardino Mountains, southern California: Constraining structural evolution. *Special Papers Geological Society of America*, p. 231-250.
- Box, S. E., Karl, S. M., Jones, J. V., III, Bradley, D. C., Haeussler, P. J., & O'Sullivan, P. B. (2019). Detrital zircon geochronology along a structural transect across the Kahiltna assemblage in the western Alaska Range: Implications for emplacement of the Alexander-Wrangellia- Peninsular terrane against North America. *Geosphere*, 15(6), p. 1774-1808. <https://doi.org/10.1130/GES02060.1>.
- Brennan, P., Gilbert, H., Ridgway, K. D. (2011). Crustal structure across the central Alaska Range: Anatomy of a Mesozoic collisional zone. *Geochemistry Geophysics Geosystems*, 12(4).
-
- Brueseke, M. E., Benowitz, J. A., Trop, J. M., Davis, K. N., Berkelhammer, S. E., Layer, P. W. and Morter, B. K. (2019). The Alaska Wrangell Arc: ~ 30 Ma of subduction-related magmatism along a still active arc-transform junction. *Terra Nova*, 31(1), p. 59-66.
- Brueseke, M. E., Benowitz, J. A., Bearden, A. T., Mann, M. E., Miggins, D. P. (2023). Subduction Disruption, Slab Tears: ca. 1 Ma true collision of a ~30-km thick oceanic plateau segment recorded by Yakutat slab nascent tear magmatism, *Terra Nova*.
- Bruhn, R. L., Sauber, J., Cotton, M. M., Pavlis, T. L., Burgess, E., Ruppert, N., & Forster, R. R. (2012). Plate margin deformation and active tectonics along the northern edge of the Yakutat Terrane in the Saint Elias Orogen, Alaska, and Yukon, Canada. *Geosphere*, 8(6), 1384-1407.
- Bruhn, R. L., Pavlis, T. L., Plafker, G., & Serpa, L. (2004). Deformation during terrane accretion in the Saint Elias orogen, Alaska. *Geological Society of America Bulletin*, 116(7-8), 771-787.

- Burkett, C. A., Bemis, S. P., and Benowitz, J. A. (2016). Along-fault migration of the Mount McKinley restraining bend of the Denali fault defined by late Quaternary fault patterns and seismicity, Denali National Park & Preserve, Alaska: *Tectonophysics*, v. 693, p. 489-506.
- Buscher, J. T. and Spotila, J. A. (2007). Near-field response to transpression along the southern San Andreas fault, based on exhumation of the northern San Gabriel Mountains, southern California. *Tectonics*, 26 (5).
- Choi, M., Eaton, D. W. and Enkelmann, E. (2021). Is the Eastern Denali fault still active?. *Geology*, 49(6), p. 662-666.
- Churkin, M., Foster, H. L., Chapman, R. M., Weber, F. R. (1982). Terranes and Suture Zones in East Central Alaska, *Journal of Geophysical Research*, Vol. 87, B5, p. 3718-3730
- Cobbett, R., Israel, S., Mortensen, J., Joyce, N., and Crowley, J., (2016). Structure and kinematic evolution of the Duke River fault, southwestern Yukon: *Canadian Journal of Earth Sciences*, v. 54, p. 322-344.
- Cole, R. B. and Ridgway, K. D. (1993). The influence of volcanism on fluvial depositional systems in a Cenozoic strike-slip basin, Denali fault system, Yukon Territory, Canada. *Journal of Sedimentary Research*, 63(1), p. 152-166.
- Cole, R. B., Ridgway, K. D., Layer, P. W. and Drake, J. (1999). Kinematics of basin development during the transition from terrane accretion to strike-slip tectonics. Late Cretaceous-early Tertiary Cantwell Formation, south central Alaska. *Tectonics*, 18(6), p.1224-1244.
- Collett, C. M., Duvall, A. R., Flowers, R. M., Tucker, G. E. and Upton, P. (2019). The timing and style of oblique deformation within New Zealand's Kaikōura Ranges and Marlborough fault System based on low-temperature thermochronology. *Tectonics*, 38(4), p. 1250-1272.
- Coney, P. J., Jones, D. L., Monger, J. W. H., 1980. Cordilleran suspect terranes. *Nature*, 288 (5789): 329-333.
- Cooke, M. L. and Madden, E. H. (2014). Is the Earth lazy? A review of work minimization in fault evolution. *Journal of Structural Geology*, 66, p. 334-346.
- Christie-Blick, N. and Biddle, K. T. (1985). Deformation and basin formation along strike-slip faults, *Basin Formation and Sedimentation*, SEPM Special Publication No. 37 p. 1-34
- Denton, G.H. and Armstrong, R.L. (1969). Miocene-Pliocene glaciations in southern Alaska. *American Journal of Science*, 267(10), p. 1121-1142.
- Donelick, R. A., O'Sullivan, P. B., & Ketcham, R. A. (2005). Apatite fission-track analysis. *Reviews in Mineralogy and Geochemistry*, 58(1), 49-94.
- Doser, D.I. (2014). Seismicity of Southwestern Yukon, Canada, and its relation to slip transfer between the Fairweather and Denali fault systems. *Tectonophysics*, 611, p. 121-129.
- Dobrovine, P. V., and Tarduno, J. A. (2008). A revised kinematic model for the relative motion between Pacific oceanic plates and North America since the Late Cretaceous: *Journal of Geophysical Research: Solid Earth*, v. 113, p. 1-20.
- Dusel-Bacon, C., Day, W. C., and Aleinikoff, J. N. (2013). Geochemistry, petrography, and zircon U-Pb geochronology of Paleozoic metagneous rocks in the Mount Veta area of east-central Alaska: Implications for the evolution of the westernmost part of the Yukon-Tanana terrane: *Canadian Journal of Earth Sciences*, v. 50, no. 8, p. 826-846, <https://doi.org/10.1139/cjes-2013-0004>.

- Duvall, A. R., Harbert, S. A., Upton, P., Tucker, G. E., Flowers, R. M. and Collett, C. (2020). River patterns reveal two stages of landscape evolution at an oblique convergent margin, Marlborough fault System, New Zealand. *Earth Surface Dynamics*, 8(1), p. 177-194.
- Eberhart-Phillips, D., Haeussler, P. J., Freymueller, J. T., Frankel, A. D., Rubin, C. M., Craw, P., Ratchkovski, N. A., Anderson, G., Carver, G. A. and Crone, A. J. (2003). The 2002 Denali fault earthquake, Alaska: a large magnitude, slip-partitioned event. *Science* 300, 1113.
- Eberhart-Phillips, D., Christensen, D. H., Brocher, T. M., Hansen, R., Rupert, N. A., Haeussler, P. J., Abers, G. A. (2006). Imaging the transition from Aleutian subduction to Yakutat collision in central Alaska, with local earthquakes and active source data, *Journal of Geophysical Research*, Vol. 111
- Eisbacher, G. H. (1976). Sedimentology of the Dezadeash flysch and its implications for strike-slip faulting along the Denali fault, Yukon Territory and Alaska. *Canadian Journal of Earth Sciences*, 13(11), p. 1495-1513. <https://doi.org/10.1139/e76-157>
- Elliott, J. L., Larsen, C. F., Freymueller, J. T., and Motyka, R. J. (2010). Tectonic block motion and glacial isostatic adjustment in southeast Alaska and adjacent Canada constrained by GPS measurements, *J. Geophys. Res.*,115, B09407, doi:10.1029/2009JB007139.
- Elliott, J., Freymueller, J. T. (2020). A Block Model of Present-Day Kinematics of Alaska and Western Canada, *J. Geophysical Research, Solid Earth*, doi: 10.1029/2019JB018378
- Engelbreton, D. C., Cox, A., and Gordon, R. G., (1985). Relative Motions Between Oceanic and Continental Plates in the Pacific Basin: Geological Society of America Special Paper 206, p. 59, <https://doi.org/10.1130/SPE206-p1>.
- Enkelmann, E., Piestrzeniewicz, A., Falkowski, S., Stübner, K. and Ehlers, T. A. (2017). Thermochronology in southeast Alaska and southwest Yukon: Implications for North American Plate response to terrane accretion. *Earth and Planetary Science Letters*, 457, p. 348-358.
- Eyles C. H., Eyles, N. (1989). The upper Cenozoic White River “Tillites” of southern Alaska: Subaerial slope and fan-delta deposits in a strike-slip setting, *Geological Society of America Bulletin*, v. 101, p. 1091-1102
- Farley, K. A. (2002). (U-Th)/He dating: Techniques, calibrations, and applications: Reviews in Mineralogy and Geochemistry, v. 47, p. 819-844, <https://doi.org/10.2138/rmg.2002.47.18>.
- Ferris, A., Abers, G.A., Christensen, D.H. and Veenstra, E., 2003. High resolution image of the subducted Pacific (?) plate beneath central Alaska, 50-150 km depth. *Earth and Planetary Science Letters*, 214 (3-4), pp.575-588.
- Finzel, E. S., Ridgway, K. D. and Trop, J. M. (2015). Provenance signature of changing plate boundary conditions along a convergent margin: Detrital record of spreading-ridge and flat-slab subduction processes, Cenozoic forearc basins, Alaska. *Geosphere*, 11(3), p. 823-849.
- Fiorillo, A. R., Adams, T. L. and Kobayashi, Y. (2012). New sedimentological, palaeobotanical, and dinosaur ichnological data on the palaeoecology of an unnamed Late Cretaceous rock unit in Wrangell-St. Elias National Park and Preserve, Alaska, USA. *Cretaceous Research*, 37, p. 291-299.
- Fitzgerald, P. G., Baldwin, S. L., Webb, L. and O’Sullivan P. (2006), Interpretation of (U-Th)/He single grain ages from slowly cooled crustal terranes: A case study from the Transantarctic Mountains of southern Victoria Land, *Chemical geology*, 225 (1-2), p. 91-120
- Fitzgerald, P. G., Malusa, M. G., Munoz, J. A. (2019). Detrital thermochronology using Conglomerates and Cobbles, in: M. G. Malusà and P. G. Fitzgerald (eds.), *Fission-Track Thermochronology and its Application to Geology*, Springer Textbooks in Earth Sciences, Geography and Environment, p. 295-314.

- Fitzgerald, P. G., Sorkhabi, R. B., Redfield, T. F. and Stump, E. (1995). Uplift and denudation of the central Alaska Range: A case study in the use of apatite fission track thermochronology to determine absolute uplift parameters. *Journal of Geophysical Research: Solid Earth*, 100(B10), p. 20175-20191.
- Fitzgerald, P. G., Stump, E. and Redfield, T. F. (1993). Late Cenozoic uplift of Denali and its relation to relative plate motion and fault morphology. *Science*, 259(5094), p.497-499.
- Fitzgerald, P. G., Roeske, S. M., Benowitz, J. A., Riccio, S. J., Perry, S. E., and Armstrong, P. A. (2014), Alternating asymmetric topography of the Alaska range along the strike-slip Denali fault: Strain partitioning and lithospheric control across a terrane suture zone: *Tectonics*, v. 33, p. 1519-1533, <https://doi.org/10.1002/2013TC003432>.
- Flowers, R. M., Zeitler, P. K., Danišik, M., Reiners, P. W., Gautheron, C., Ketcham, R. A., and Brown, R. W. (2023a). (U-Th)/He chronology: Part 1. Data, uncertainty, and reporting. *Bulletin*, 135(1-2), 104-136.
- Flowers, R. M., Ketcham, R. A., Enkelmann, E., Gautheron, C., Reiners, P. W., Metcalf, J. R., and Brown, R. W. (2023b). (U-Th)/He chronology: Part 2. Considerations for evaluating, integrating, and interpreting conventional individual aliquot data. *Bulletin*, 135(1-2), 137-161.
- Forbes, R. B., Smith, T. E., & Turner, D. L. (1974). Comparative petrology and structure of the Maclaren, Ruby Range, and Coast Range belts: Implications for offset along the Denali fault system. *Geological Society of America Abstracts with Programs*. 6, 177.
- Gallagher K., Brown R., Johnson C. (1998). Fission track analysis and its applications to geological problems. *Ann Rev Earth Planet Sci* 26:519-572.
- Gleadow, A.J.W., 1981, Fission--Track dating methods: What are the real alternates? *Nuclear Tracks*, v. 5, no. 1/2, p. 3-14.
- Gleadow, A. J. W., Duddy, I. R., Lovering, J. F. (1983). Fission track analysis: a new tool for the evaluation of thermal histories and hydrocarbon potential. *Aust Pet Explor Assoc J* 23:92-102
- Gleadow A. J. W., Duddy I. R., Green P. F., Lovering J.F. (1986). Confined fission track lengths in apatite: a diagnostic tool for thermal history analysis. *Contrib Miner Petrol* 94, p. 405-415
- Gleadow A. J. W., Fitzgerald P. G. (1987). Uplift history and structure of the Transantarctic Mountains: new evidence from fission track dating of basement apatites in the Dry Valleys area, southern Victoria Land. *Earth Planet Sci Lett* 82, p. 1-14
- Gulick, S. P. S., Reece, R. S., Christeson, G. L., Van Avendonk, H., Worthington, L. L. and Pavlis, T. L. (2013). Seismic images of the Transition fault and the unstable Yakutat-Pacific-North American triple junction. *Geology*, 41(5), p. 571-574.
- Haeussler, P. J., Matmon, A., Schwartz, D. P., and Seitz, G. G. (2017). Neotectonics of interior Alaska and the late Quaternary slip rate along the Denali fault system: *Geosphere*, v. 13, p. 1445-1463
- Haeussler, P. J., O'sullivan, P., Berger, A. L. and Spotila, J. A. (2008). Neogene exhumation of the Tordrillo Mountains, Alaska, and correlations with Denali (Mount McKinley). *Washington DC American Geophysical Union Geophysical Monograph Series*, 179, p. 269-285.
- Haeussler, P. J., Schwartz, D. P., Dawson, T. E., Stenner, H. D., Lienkaemper, J. J., Sherrod, B., Cinti, F. R., Montone, P., Craw, P. A., Crone, A. J., Personius, S. F. (2004). Surface rupture and slip distribution of the Denali and Totschunda faults in the 3 November 2002 M7.9 Earthquake, Alaska, *Bulletin Seismology Society of America*, v. 94, p. 23-52
- Hiess, J., Condon, D. J., Mclean, N., and Noble, S. R. (2012). U-238/U-235 Systematics in Terrestrial Uranium-Bearing Minerals: *Science*, v. 335, p. 1610-1614

- Huntington, K. W., Blythe, A. E., Hodges, K. V. (2006). Climate change and late Pliocene acceleration of erosion in the Himalaya, *Earth and Planetary science letters*, V. 252 p 107-118
- Hurford, A.J., Green, P.F., 1983, The zeta calibration of fission track dating. *Isotope geoscience*, 1, p. 285-317
- Jicha, B. R., Garcia, M. O., & Wessel, P. (2018). Mid-Cenozoic Pacific plate motion change: Implications for the northwest Hawaiian Ridge and circum-Pacific. *Geology*, 46 (11), 939-942.
- Johnson, J. E., Flowers, R. M., Baird, G. B. and Mahan, K. H. (2017). “Inverted” zircon and apatite (U-Th)/He dates from the Front Range, Colorado: high-damage zircon as a low-temperature (< 50deg C) thermochronometer. *Earth and Planetary Science Letters*, 466, p. 80-90.
- Jones, D., Siberling, N., Gilbert, W., and Coney, P. (1982). Character, distribution, and tectonic significance of accretionary terranes in the central Alaska Range: *Journal of Geophysical Research: Solid Earth*, v. 87, p. 3709-3717
- Jones III, J. V., Todd, E., Box, S. E., Haeussler, P. J., Holm-Denoma, C. S., Karl, S. M., Graham, G. E., Bradley, D. C., Kylander-Clark, A. R., Friedman, R. M. and Layer, P. W. (2021). Cretaceous to Oligocene magmatic and tectonic evolution of the western Alaska Range: Insights from U-Pb and 40Ar/39Ar geochronology. *Geosphere*, 17(1), p. 118-153.
- Jones, J., Caine, J., Holm-Denoma, C., Ryan, J., Benowitz, J., and Drenth, B. (2017). Unraveling the boundary between the Yukon-Tanana terrane and the parautochthonous North America in eastern Alaska: *Geological Society of America Abstracts with Programs*, v. 49, no. 6
- Kaufman, D.S., Young, N.E., Briner, J.P. and Manley, W.F. (2011). Alaska palaeo-glacier atlas In *Developments in Quaternary Sciences* (Vol. 15, pp. 427-445). Elsevier.
- Kellogg, K. S., Minor, S. A. (2005). Pliocene transpressional modification of depositional basins by convergent thrusting adjacent to the “Big Bend” of the San Andreas fault: An example from Lockwood Valley, southern California. *Tectonics*, 24(1).
- Ketcham, R. A., (2003). Observations on the relationship between crystallographic orientation and biasing in apatite fission-track measurements. *American Mineralogist*, 88(5-6), p. 817-829.
- Ketcham, R. A., (2005). Forward and Inverse Modeling of Low Temperature Thermochronometry Data, *Reviews in Mineralogy and Geochemistry*, Vol. 58, p 278-314
- Ketcham, R. A., Carter, A., Donelick, R. A., Barbarand, J. and Hurford, A. J. (2007). Improved modeling of fission-track annealing in apatite. *American Mineralogist*, 92(5-6), p. 799-810.
- Ketcham, R. A., Gautheron, C., & Tassan-Got, L. (2011). Accounting for long alpha-particle stopping distances in (U-Th-Sm)/He geochronology: Refinement of the baseline case. *Geochimica et Cosmochimica Acta*, 75(24), p. 7779-7791. <http://doi.org/10.1016/j.gca.2011.10.011>
- Lahr, J. C., & Plafker, G. (1980). Holocene Pacific–North American plate interaction in southern Alaska: Implications for the Yakataga seismic gap. *Geology*, 8(10), 483-486.
- Lease, R.O., Haeussler, P.J., and O’Sullivan, P., (2016). Changing exhumation patterns during Cenozoic growth and glaciation of the Alaska Range: Insights from detrital thermochronology and geochronology: *Tectonics*, v. 35, p. 934-955
- Lease, R. O., Haeussler, P. J., Witter, R. C., Stockli, D. F., Bender, A. M., Kelsey, H. M., O’Sullivan, P.B. (2021). Extreme Quaternary plate boundary exhumation and strike-slip localized along the southern Fairweather fault, Alaska, USA. *Geology*, 49(5), p. 602-606.

- Lowey, G. W. (2019). Provenance analysis of the Dezadeash Formation (Jurassic-Cretaceous), Yukon, Canada: Implications regarding a linkage between the Wrangellia composite terrane and the western margin of Laurasia. *Canadian Journal of Earth Sciences*, 56(1), p. 77-100. <https://doi.org/10.1139/cjes-2017-0244>
- Lozos, J. C. (2016). A case for historic joint rupture of the San Andreas and San Jacinto faults. *Science advances*, 2(3), p.e1500621.
- Ludwig, K. R. (1998). On the treatment of concordant uranium-lead ages. *Geochimica et Cosmochimica Acta*, 62(4), p.665-676.
- MacKevett, E. M. (1978). *Geologic Map of the McCarthy Quadrangle, Alaska: U.S. Geological Survey Miscellaneous Investigation Series I-1032, scale 1:250,000.*
- Mann, M. E., Abers, G. A., Daly, K., Christensen, D. H. (2022). Subduction of an Oceanic Plateau Across Southcentral Alaska: Scattered-Wave Imaging. *Journal of Geophysical Research: Solid Earth*: e2021JB022697.
- Manselle, P., Brueseke, M. E., Trop, J. M., Benowitz, J. A., Snyder, D. C., and Hart, W. K. (2020). Geochemical and stratigraphic analysis of the Chisana Formation, Wrangellia terrane, eastern Alaska: Insights into Early Cretaceous magmatism and tectonics along the northern Cordilleran margin: *Tectonics*, v. 39, no. e2020TC006131.
- Marechal, A., Ritz, J. F., Ferry, M., Mazzotti, S., Blard, P. H., Braucher, R. and Saint-Carlier, D. (2018). Active tectonics around the Yakutat indenter: New geomorphological constraints on the eastern Denali, Totschunda and Duke River faults. *Earth and Planetary Science Letters*, 482, p.71-80.
- Marincovich, L. and Gladenkov, A. Y. (1999). Evidence for an early opening of the Bering Strait. *Nature*, 397 (6715), p. 149-151.
- Matmon, A., Schwartz, D. P., Haeussler, P. J., Finkel, R., Lienkaemper, J. J., Stenner, H. D. and Dawson, T. E. (2006). Denali fault slip rates and Holocene-late Pleistocene kinematics of central Alaska. *Geology*, 34(8), p. 645-648.
- McAleer, R. J., Spotila, J. A., Enkelmann, E. and Berger, A. L. (2009). Exhumation along the Fairweather fault, southeastern Alaska, based on low-temperature thermochronometry. *Tectonics*, 28(1).
- McBeck, J., Cooke, M. and Madden, E. (2017). Work optimization predicts the evolution of extensional step overs within anisotropic host rock: Implications for the San Pablo Bay, CA. *Tectonics*, 36(11), p.2630-2646.
- McCaffrey, R., Zwick, P. C., Bock, Y., Prawirodirdjo, L., Genrich, J. F., Stevens, C. W., Puntodewo, S. S. O., Subarya, C. (2000). Strain partitioning during oblique plate convergence in northern Sumatra: Geodetic and seismologic constraints and numerical modeling, *Journal of Geophysical Research*, Vol. 105, No. B12, p 363-376
- McDermott, R. G., Ault, A. K., Caine, J. S. and Thomson, S. N. (2019). Thermotectonic history of the Kluane Ranges and evolution of the eastern Denali fault zone in southwestern Yukon, Canada. *Tectonics*, 38(8), p. 2983-3010.
- McDermott, R. G, Ault, A. K., Caine, J. S. (2021). Dating fault damage along the eastern Denali fault zone with hematite (U-Th)/He thermochronometry, *Earth and Planetary science Letters* 563
- McGeary, S., Nur, A., & Ben-Avraham, Z. (1985). Spatial gaps in arc volcanism: The effect of collision or subduction of oceanic plateaus. *Tectonophysics*, 119(1-4), p. 195-221.
- Milde, E. R. (2014), *Using Low-Temperature Thermochronology to Constrain the Role of the Totschunda fault in Southeastern Alaskan Tectonics [M.S. thesis]: Syracuse, New York, Syracuse University, 127 p.*

- Miller, M. L., Bradley, D. C., Bundtzen, T. K., and McClelland, W. (2002) Late Cretaceous through Cenozoic strike-slip tectonics of southwestern Alaska: *The Journal of Geology*, v. 110, p. 247-270
- Mukasa, S. B., Andronikov, A. V. and Hall, C. M. (2007). The $^{40}\text{Ar}/^{39}\text{Ar}$ chronology and eruption rates of Cenozoic volcanism in the eastern Bering Sea Volcanic Province, Alaska. *Journal of Geophysical Research: Solid Earth*, 112(B6).
- Nabelek, P. I., Hofmeister, A. M., & Whittington, A. G. (2012). The influence of temperature-dependent thermal diffusivity on the conductive cooling rates of plutons and temperature-time paths in contact aureoles. *Earth and Planetary Science Letters*, 317, 157-164.
- Najman, Y., Sobel, E. R., Millar, I., Luan, X., Zapata, S., Garzanti, E., Parra, M., Vezzoli, G., Zhang, P., Wa Aung, D. and Paw, S. M. T. L. (2022). The timing of collision between Asia and the West Burma Terrane, and the development of the Indo-Burman Ranges. *Tectonics*, 41(7), p.e2021TC007057.
- Nokleberg, W. J., Jones, D. L., & Silberling, N. J. (1985). Origin and tectonic evolution of the Maclaren and Wrangellia terranes, eastern Alaska Range, Alaska. *The Geological Society of America Bulletin*, 96(10), p. 1251-1270
- Nokleberg, W. J., & Richter, D. H. (2007). Origin of narrow terranes and adjacent major terranes occurring along the Denali fault in the Eastern and Central Alaska Range, Alaska. In K. D. Ridgway, J. M. Trop, J. M. G. Glen, & J. M. O'Neill (Eds.), *Special Paper 431: Tectonic growth of a collisional continental margin: Crustal evolution of southern Alaska*, Vol. 431, p. 129-154
- Oglesby, D.D., Dreger, D.S., Harris, R.A., Ratchkovski, N. and Hansen, R. (2004). Inverse kinematic and forward dynamic models of the 2002 Denali fault earthquake, Alaska. *Bulletin of the Seismological Society of America*, 94(6B), pp.S214-S233
- Passchier, C.W. and Platt, J.P. (2017). Shear zone junctions: Of zipers and freeways. *Journal of Structural Geology*, 95, p. 188-202.
- Paton, C., Woodhead, J. D., Hellstrom, J. C., Hergt, J. M., Greig, A., and Maas, R. (2010). Improved laser ablation U-Pb zircon geochronology through robust downhole fractionation correction, *Geochem. Geophys. Geosyst.*, 11
- Powell, R.E. (1993). "Chapter 1: Balanced palinspastic reconstruction of pre-late Cenozoic paleogeology, southern California: Geologic and kinematic constraints on evolution of the San Andreas fault system", *The San Andreas fault System: Displacement, Palinspastic Reconstruction, and Geologic Evolution*, Robert E. Powell, R. J. Weldon, II, Jonathan C. Matti
- Pavlis, G. L., Bauer, M. A., Elliot, J. L., Koons, P., Pavlis, T. L., Ruppert, N., Ward, K. M., Worthington, L. L. (2019). A unified three-dimensional model of the lithospheric structure at the subduction corner in southeast Alaska: Summary results from STEEP, *Geosphere*, v. 15., p. 382-406. <https://doi.org/10.1130/GES01488.1>
- Raymo, M. E. (1994). The initiation of Northern Hemisphere glaciation. *Annual Review of Earth and Planetary Sciences*, 22(1), p. 353-383.
- Redfield, T. and Fitzgerald, P. (1993). Denali fault system of southern Alaska: an interior strike-slip structure responding to dextral and sinistral shear coupling. *Tectonics* 12, p. 1195-1208.
- Reece, R. S., Gulick, S. P., Christeson, G. L., Horton, B. K., van Avendonk, H., Barth, G. (2013). The role of farfield tectonic stress in oceanic intraplate deformation, Gulf of Alaska. *Journal of Geophysical Research: Solid Earth*, 118(5), p. 1862-1872.
- Regan, S. P., Benowitz, J. A., Waldien, T. S., Holland, M. E., Roeske, S. M., O'Sullivan, P., Layer, P. (2021). Long distance plutonic relationships demonstrate 33 million years of strain partitioning along the Denali fault. *Terra Nova*, 33(6), p. 630-640.

- Regan, S. P., Benowitz, J. A., and Holland, M. E. (2020). A plutonic brother from another magma mother: Disproving the Eocene Foraker-McGonagall pluton piercing point and implications for long-term slip on the Denali fault: *Terra Nova*, v. 32, p. 66-74
- Riccio, S. J., Fitzgerald, P. G., Benowitz, J. A., and Roeske, S. M. (2014). The role of thrust faulting in the formation of the eastern Alaska Range: Thermochronological constraints from the Susitna Glacier thrust fault region of the intracontinental strike-slip Denali fault system: *Tectonics*, v. 33, p. 2195-2217, <https://doi.org/10.1002/2014TC003646>.
- Richter, D.H. and Matson Jr, N.A. (1971). Quaternary faulting in the eastern Alaska Range. *Geological Society of America Bulletin*, 82(6), p. 1529-1540.
- Richter, D. H., (1976). *Geologic Map of the Nabesna Quadrangle: U.S. Geological Survey Miscellaneous Geologic Investigations Map I-932, scale 1:250,000.*
- Richter, D. H., Smith, J. G., Lanphere, M. A., Dalrymple, G. B., Reed, B. L., Shew, N. (1990). Age and progression of volcanism, Wrangell volcanic field, Alaska: *Bulletin of Volcanology*, v. 53, p. 29-44
- Ridgway, K. D., Decelles, P. G. (1993). Stream-dominated alluvial fan and lacustrine depositional systems in Cenozoic strike-slip basins, Denali fault system, Yukon Territory, Canada. *Sedimentology*, 40(4), p. 645-666.
- Ridgway, K. D., Trop, J. M., Nokleberg, W. J., Davidson, C. M. and Eastham, K. R. (2002). Mesozoic and Cenozoic tectonics of the eastern and central Alaska Range: Progressive basin development and deformation in a suture zone. *Geological Society of America Bulletin*, 114 (12), p. 1480-1504.
- Rivera, T. A., Storey, M., Zeeden, C., Hilgen, F. J., and Kuiper, K. (2011). A refined astronomically calibrated $40\text{Ar}/39\text{Ar}$ age for Fish Canyon sanidine: *Earth and Planetary Science Letters*, v. 311, no. 3-4, p. 420-426
- Rosenthal, J., Betka, P., Nadin, E., Gillis, R., and Benowitz, J. (2018), Vein formation during progressive Paleogene faulting and folding within the lower Cook Inlet basin, Alaska: *Geosphere*, v. 14, no. 1, p. 23-49, <http://doi.org/10.1130/GES01435.1>.
- Rossi, G., Abers, G. A., Rondenay, S. and Christensen, D. H. (2006). Unusual mantle Poisson's ratio, subduction, and crustal structure in central Alaska. *Journal of Geophysical Research: Solid Earth*, 111 (B9).
-
- Schwartz, D. P., Haeussler, P. J., Seitz, G. G., Dawson, T. E. (2012). Why the 2002 Denali fault rupture propagated onto the Totschunda fault: Implications for fault branching and seismic hazards. *Journal of Geophysical Research: Solid Earth*, 117(B11).
- Skulski, T., Francis, D., & Ludden, J. (1992). Volcanism in an arc-transform transition zone: The stratigraphy of the St. Clare Creek volcanic field, Wrangell volcanic belt, Yukon, Canada. *Canadian Journal of Earth Sciences*, 29, p. 446-461.
- Spencer, C. J., Kirkland, C. L., & Taylor, R. J. (2016). Strategies towards statistically robust interpretations of in situ U-Pb zircon geochronology. *Geoscience Frontiers*, 7(4), p. 581-589.
- Spotila, J. A., Farley, K. A., Yule, J. D., Reiners, P. W. (2001). Near-field transpressive deformation along the San Andreas fault zone in southern California, based on exhumation constrained by (U-Th)/He dating. *Journal of Geophysical Research*, 106(B12): 30909.
- Spotila, J. A., Niemi, N., Brady, R., House, M., Buscher, J. and Oskin, M. (2007). Long-term continental deformation associated with transpressive plate motion: The San Andreas fault. *Geology*, 35(11), p. 967-970.

- Spotila, J. A., Berger, A. L. (2010). Exhumation at Orogenic Indentor Corners under Long-Term Glacial Conditions: Example of the St. Elias Orogen, Southern Alaska. *Tectonophysics*, 490, p. 241-256.
- Spotila, J. A., Farley, K. A. and Sieh, K. (1998). Uplift and erosion of the San Bernardino Mountains associated with transpression along the San Andreas fault, California, as constrained by radiogenic helium thermochronometry. *Tectonics*, 17(3), p. 360-378.
- Storti F., Holdsworth, R. E., Salvani, F. (2003). Intraplate Strike-Slip Deformation Belts. Geological Society Special Publication, 210
- Sylvester, A. G. (1988). Strike-slip faults. *Geological Society of America Bulletin*, 100, p. 1666-1703.
- Townsend, K. F., Clark, M. K. and Niemi, N. A. (2021). Reverse faulting Within a Continental Plate Boundary Transform System. *Tectonics*, 40(11), e2021TC006916.
- Trop, J. M., Benowitz, J. A., Kirby, C. S. and Brueseke, M. E. (2022). Geochronology of the Wrangell Arc: Spatial-temporal evolution of slab-edge magmatism along a flat-slab, subduction-transform transition, Alaska-Yukon. *Geosphere*, 18(1), p. 19-48.
- Trop, J. M., Benowitz, J., Cole, R. B. and O'Sullivan, P. (2019). Cretaceous to Miocene magmatism, sedimentation, and exhumation within the Alaska Range suture zone: A polyphase reactivated terrane boundary. *Geosphere*, 15(4), p. 1066-1101.
- Trop, J.M., and Ravn, R.L. (2003). Sedimentology, palynology, and petrology of the Cretaceous Matanuska Formation, south-central Alaska: Relationships between forearc basin development and accretionary tectonic events: *Geological Society of America Abstracts with Programs*, v. 35, no. 6, p. 559.
- Trop, J.M., and Ridgway, K.D. (2007). Mesozoic and Cenozoic tectonic growth of southern Alaska: A sedimentary basin perspective, in Ridgway, K.D., Trop, J.M., Glen, J.M.G., and O'Neill, J.M., eds., *Tectonic Growth of a Collisional Continental Margin: Crustal Evolution of Southern Alaska: Geological Society of America Special Paper 431*, p. 55-94
- Trop, J. M., Hart, W. K., Snyder, D. and Idleman, B. (2012). Miocene basin development and volcanism along a strike-slip to flat-slab subduction transition: Stratigraphy, geochemistry, and geochronology of the central Wrangell volcanic belt, Yakutat-North America collision zone. *Geosphere*, 8(4), p.805-834.
- Wahrhaftig, C. (1975). Late Cenozoic orogeny in the central Alaska Range (abstract), *Spec. Pap. Geol. Soc. Am.*, 151, p. 189-190
- Walcott, R. I. (1998). Modes of oblique compression: Late Cenozoic tectonics of the South Island of New Zealand. *Reviews of Geophysics*, 36(1), p. 1-26.
- Waldien, T. S., Roeske, S. M. and Benowitz, J. A. (2021a). Tectonic Underplating and Dismemberment of the Maclaren-Kluane Schist Records Late Cretaceous Terrane Accretion Polarity and ~ 480 km of Post-52 Ma Dextral Displacement on the Denali fault. *Tectonics*, 40(10)
- Waldien, T. S., Roeske, S. M., Benowitz, J. A., Twelker, E., and Miller, M. S. (2021b). Oligocene-Neogene lithospheric-scale reactivation of Mesozoic terrane accretionary structures in the Alaska Range suture zone, southern Alaska, USA: *Geological Society of America Bulletin*, v. 133, p. 691-716
- Waldien, T. S., Roeske, S. M., Benowitz, J. A., Allen, W. K., Ridgway, K. D. and O'Sullivan, P. B. (2018). Late Miocene to Quaternary evolution of the McCallum Creek thrust system, Alaska: Insights for range-boundary thrusts in transpressional orogens. *Geosphere*, 14(6), p. 2379-2406.
- Waldien, T. S., Lease, R. O., Roeske, S. M., Benowitz, J. A. and O'Sullivan, P. B. (2022). The role of preexisting upper plate strike-slip faults during long-lived (ca. 30 Myr) oblique flat slab subduction, southern Alaska. *Earth and Planetary Science Letters*, 577

White, S. H. and Green, P. F. (1986). Tectonic development of the Alpine fault zone, New Zealand: A fission-track study. *Geology*, 14(2), p. 124-127.

Wilson, F. H., Hults, C. P., Mull, C. G., and Karl, S. M. (2015). Geologic Map of Alaska: U.S. Geological Survey Scientific Investigations Map 3340, scale 1:1,584,000, 2 sheets

Wilson, J. T. (1968). Static or Mobile earth and the Current Scientific Revolution, *Proceedings of the American Philosophical Society*, Vol. 112, No. 5

Wolf, R. A., Farley, K. A. and Silver, L. T. (1996). Helium diffusion and low-temperature thermochronometry of apatite. *Geochimica et Cosmochimica Acta*, 60(21), p.4231-4240.

Worthington, L. L., Van Avendonk, H. J., Gulick, S. P., Christeson, G. L. and Pavlis, T. L. (2012). Crustal structure of the Yakutat terrane and the evolution of subduction and collision in southern Alaska. *Journal of Geophysical Research: Solid Earth*, 117